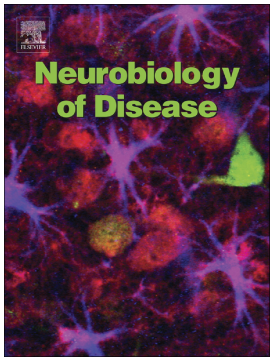

Dopamine-iron homeostasis interaction rescues mitochondrial fitness in Parkinson's disease

Chiara Buoso, Markus Seifert, Martin Lang, Corey M. Griffith, Begoña Talavera Andújar, Maria Paulina Castelo Rueda, Christine Fischer, Carolina Doerrier, Heribert Talasz, Alessandra Zanon, Peter P. Pramstaller, Emma L. Schymanski, Irene Pichler, Guenter Weiss

PII: S0969-9961(24)00105-0

DOI: https://doi.org/10.1016/j.nbd.2024.106506

Reference: YNBDI 106506

To appear in: *Neurobiology of Disease*

Received date: 21 December 2023

Revised date: 17 April 2024

Accepted date: 17 April 2024

Please cite this article as: C. Buoso, M. Seifert, M. Lang, et al., Dopamine-iron homeostasis interaction rescues mitochondrial fitness in Parkinson's disease, *Neurobiology of Disease* (2023), https://doi.org/10.1016/j.nbd.2024.106506

Dopamine-iron homeostasis interaction rescues mitochondrial fitness in Parkinson's disease

Chiara Buoso[a,b], Markus Seifert[b,c], Martin Lang[a], Corey M. Griffith[d], Begoña Talavera Andújar[d], Maria Paulina Castelo Rueda[a], Christine Fischer[b], Carolina Doerrier[f], Heribert Talasz[e], Alessandra Zanon[a], Peter P. Pramstaller[a], Emma L. Schymanski[d], Irene Pichler[a*], Guenter Weiss[b,c*]

[a] *Institute for Biomedicine, Eurac Research, 39100 Bolzano, Italy.*

[b] *Department of Internal Medicine II, Medical University of Innsbruck, 6020 Innsbruck, Austria.*

[c] *Christian Doppler Laboratory for Iron Metabolism and Anemia Research, Medical University of Innsbruck, 6020 Innsbruck, Austria.*

[d] *Luxembourg Centre for Systems Biomedicine (LCSB), University of Luxembourg, 4362 Belvaux, Luxembourg.*

[e] *Institute of Medical Biochemistry, Protein Core Facility, Biocenter Innsbruck, Medical University of Innsbruck, 6020 Innsbruck, Austria.*

[f] *Oroboros Instruments, 6020 Innsbruck, Austria.*

*These authors have contributed equally

Address correspondence to: irene.pichler@eurac.edu; Guenter.Weiss@i-med.ac.at

ABSTRACT

Imbalances of iron and dopamine metabolism along with mitochondrial dysfunction have been linked to the pathogenesis of Parkinson's disease (PD). We have previously suggested a direct link between iron homeostasis and dopamine metabolism, as dopamine can increase cellular uptake of iron into macrophages thereby promoting oxidative stress responses. In this study, we investigated the interplay between iron, dopamine, and mitochondrial activity in neuroblastoma SH-SY5Y cells and human induced pluripotent stem cell (hiPSC)-derived dopaminergic neurons differentiated from a healthy control and a PD patient with a mutation in the α-synuclein (*SNCA*) gene. In SH-SY5Y cells, dopamine treatment resulted in increased expression of the transmembrane iron transporters transferrin receptor 1 (TFR1), ferroportin (FPN), and mitoferrin2 (MFRN2) and intracellular iron accumulation, suggesting that dopamine may promote iron uptake. Furthermore, dopamine supplementation led to reduced mitochondrial fitness including decreased mitochondrial respiration, increased cytochrome *c* control efficiency, reduced mtDNA copy number and citrate synthase activity, increased oxidative stress and impaired aconitase activity. In dopaminergic neurons derived from a healthy control individual, dopamine showed comparable effects as observed in SH-SY5Y cells. The hiPSC-derived PD neurons harboring an endogenous *SNCA* mutation demonstrated altered mitochondrial iron homeostasis, reduced mitochondrial capacity along with increased oxidative stress and alterations of tricarboxylic acid cycle linked metabolic pathways compared with control neurons. Importantly, dopamine treatment of PD neurons promoted a rescue effect by increasing mitochondrial respiration, activating antioxidant stress response, and normalizing altered metabolite levels linked to mitochondrial function. These observations provide evidence that dopamine affects iron homeostasis, intracellular stress responses and mitochondrial function in healthy cells, while dopamine supplementation can restore the disturbed regulatory network in PD cells.

Keywords:

Parkinson's disease; iron; dopamine; mitochondrial function; hiPSC-derived neurons;

Abbreviations: PD: Parkinson's disease; hiPSCs: human induced pluripotent stem cells; TFR1: transferrin receptor 1; DMT1: divalent metal transporter 1; FPN: ferroportin; MFRN2: mitoferrin2; FTH: ferritin; PGC-1α: peroxisome proliferator-activated receptor gamma coactivator-1α ; ACO2: aconitase 2; 3-NT: nitrotyrosine; FTMT: mitochondrial ferritin; mtDNA: mitochondrial DNA; ROS: reactive oxygen species; α-syn: α-synuclein; qRT-PCR: real time PCR; LC-HRMS: liquid chromatography-high resolution mass spectrometry; AAS: atomic absorption spectroscopy; OCR: oxygen consumption rate; HRR: high-resolution respirometry; *FCR*: flux

control ratio; FCCP: carbonyl cyanide-p-trifluoromethoxy phenyl hydrazone; $FeCl_3$: ferric chloride; DFO: deferoxamine

Introduction

Parkinson's disease (PD) is the second most common neurodegenerative disease after Alzheimer's disease. PD is mostly an age-related disease, with incidence and prevalence increasing sharply with age (Collaborators, 2018; Pringsheim et al., 2014). The mean age of onset of PD is in the early-to-mid 60s, while early-onset PD refers to the minority of cases in which PD is diagnosed before 40 years of age (Bloem et al., 2021; Post et al., 2020). PD is characterized by dopaminergic neuronal loss in the *substantia nigra pars compacta* (*SNpc*), the formation of intracytoplasmic proteinaceous inclusions known as Lewy bodies (LBs), and iron accumulation (Forno, 1996; Jellinger et al., 1990; Riederer et al., 1989; Spillantini et al., 1998). Most PD cases are considered idiopathic (~ 90%), and about 10% represent PD cases caused by mutations in single genes (Chang et al., 2017; Marras et al., 2016). Mutations in *SNCA, LRRK2, PRKN, PINK1,* and *DJ-1*, among others, cause PD or early-onset forms of the disease (Blauwendraat et al., 2020). Point mutations and gene multiplications (duplication, triplication) in the *SNCA* gene encoding the α-synuclein protein (α-syn) cause severe forms of parkinsonism resulting in α-syn accumulation, oligomerization into fibrils, and LB formation (Chartier-Harlin et al., 2004; Shibasaki et al., 1995). α-syn accumulation is one of the molecular hallmarks of PD, together with mitochondrial dysfunction, oxidative stress and altered iron homeostasis (Bernal-Conde et al., 2019; Kaindlstorfer et al., 2018; Ma et al., 2021; Malpartida et al., 2021). Substantial evidence suggests that the mitochondrial electron transfer system, particularly Complex I (NADH:ubiquinone oxidoreductase) activity, is impaired in PD (Grunewald et al., 2019; Park et al., 2018). Moreover, mitochondrial DNA (mtDNA) alterations as well as mutations in genes involved in mitochondrial function (e.g. *PRKN*, *PINK1, SNCA*) can interfere with normal cell metabolism or cause rare genetic forms of the disease (Antonyova et al., 2020; Lang et al., 2022; Zanon et al., 2017). Specifically, a functional association between α-syn and mitochondrial membranes has been observed, with data suggesting that this interaction might induce α-syn accumulation and mitochondrial dysfunction (Choi et al., 2022; Monzio Compagnoni et al., 2020). Furthermore, oxidative damage takes part in the cascade of events leading to dopaminergic neurodegeneration in PD. Several sources can generate reactive oxygen species (ROS) within a cell, including interactions between redox-active metals, like iron, and oxygen species (Fenton and Haber-Weiss reactions) and activation of enzymes, such as nitric oxide synthase or NADPH oxidases (Dias et al., 2013; Koskenkorva-Frank et al., 2013), mediated by metals. Also, enzymatic oxidation or auto-oxidation of dopamine itself are recognized as causes of oxidative stress. Dopamine and its metabolites contain two hydroxyl residues that can induce cytotoxicity in dopaminergic neurons by producing highly reactive dopamine and DOPA quinones (Miyazaki and Asanuma, 2008). Outside of synaptic vesicles, dopamine is less stable and more prone to be metabolized via monoamine oxidase (MAO) or to auto-oxidize, resulting in the formation of cytotoxic ROS and neuromelanin

(Sulzer et al., 2000), which can be protective or harmful depending on the amount of iron bound to it (Zucca et al., 2017). High levels of iron favor oxidative stress and therefore play a crucial role in the development of neurodegenerative diseases such as PD (Li et al., 2016; Ma et al., 2021).

Iron deposition was first observed in a PD brain by Lhermitte and colleagues in 1924 (Lhermitte et al., 1924), and it is still not clear whether this is a cause or a consequence of the disease process. However, iron accumulation in PD might be related to dopamine homeostasis (Hare and Double, 2016), and a disequilibrium between dopamine, iron and neuromelanin might trigger degeneration of dopaminergic neurons (Zucca et al., 2017). Furthermore, a correlation between iron overload in the brain, α-syn accumulation (Joppe et al., 2019; Ortega et al., 2016), and mitochondrial dysfunction (Munoz et al., 2016; Parihar et al., 2008) has been established. Iron metabolism is tightly regulated at systemic and cellular levels (Gao et al., 2019). Under physiological conditions, iron is an essential co-factor for metabolic processes, mitochondrial respiration, oxygen transport, and DNA synthesis or repair (Cheng et al., 2022; Cronin et al., 2019; Muckenthaler et al., 2017). In mitochondria, iron is necessary for heme synthesis, iron-sulfur (Fe-S) cluster biogenesis and can be stored in mitochondrial ferritin (Lane et al., 2015; Lill and Freibert, 2020). In the brain, iron is required for mitochondrial respiration and energy production, DNA replication, myelin synthesis, and as a co-factor of iron-containing enzymes like tyrosine hydroxylase and phenylalanine hydroxylase for neurotransmitter synthesis (dopamine, norepinephrine, and serotonin) (Cheng et al., 2022). Changes in iron status are known to regulate the dopaminergic system leading to or aggravating neurodegeneration (Ci et al., 2020; Matak et al., 2016). Because neuronal mitochondrial respiration is responsible for about 20% of the body's oxygen consumption, the maintenance of physiological iron levels is critical for proper brain activity. Indeed, under physiological conditions, iron and dopamine collaborate for normal brain functioning, while under pathological conditions they can constitute a toxic couple (Hare and Double, 2016).

We have previously suggested a direct link between cellular iron homeostasis and dopamine metabolism, as dopamine can increase cellular uptake of iron into macrophages *in vitro* and *in vivo,* also promoting oxidative stress responses (Dichtl et al., 2019; Dichtl et al., 2018). Further, we have demonstrated that in subjects with restless legs syndrome, a neurological disease with indication of mitochondrial iron deficiency responding to dopaminergic medication like Levodopa, treatment with Levodopa resulted in improved mitochondrial function (Haschka et al., 2019). Based on these observations, we set out to further clarify the interaction of dopamine and iron in the context of PD by investigating the effect of dopamine on iron homeostasis, mitochondrial function and ROS production in neuroblastoma SH-SY5Y cells and PD-specific human neuronal models. We provide evidence that dopamine affects cellular iron trafficking, intracellular stress responses and mitochondrial function in neuronal cells. This regulatory network is compromised in PD cells but can be restored upon dopamine supplementation.

Material and methods

Cell lines and culture conditions

Neuroblastoma SH-SY5Y cells (ATCC, CRL-2266™) were cultured in Dulbecco's modified Eagle's Medium/Nutrient Mixture F-12+GlutaMAX™ supplement (DMEM/F12) (Thermo Fisher Scientific, 10565018) supplemented with 10 % fetal bovine serum and 1 % penicillin-streptomycin (Thermo Fisher Scientific, 15070-063). To test enhanced neuronal properties, undifferentiated SH-SY5Y cells were differentiated using retinoic acid and cholesterol (Cheung et al., 2009, Teppola et al., 2016). Human induced pluripotent stem cells (hiPSCs) from a control individual (hiPSC-SFC084-03-02, CTRL, female, age at biopsy: 63) and a PD patient with a triplication mutation of the *SNCA* gene (hiPSC-ND34391, 3x*SNCA*, female, age at biopsy: 55) were used. hiPSC-SFC084-03-02 was established through the StemBANCC consortium (https://cells.ebisc.org/STBCi033-B/), while hiPSC-ND34391 was obtained from the Coriell Cell Repository. Both lines were shared with the Institute for Biomedicine (Eurac Research) under MTA for research purposes. The study was approved by the Ethics Committee of the South Tyrolean Health Care System (approval number 102/2014 dated 26/11/2014 with extension dated 19/02/2020).

hiPSCs were cultured in mTeSR1 culture medium (Stem Cell Technologies, 85850) plus mTeSR1 supplement (Stem Cell Technologies, 85850) with 1 % Penicillin-Streptomycin (P/S) (Thermo Fisher Scientific, 15070-063) on Matrigel (Corning) coated plates under feeder-free conditions. hiPSC colonies were split every 3-4 days at a ratio of 1:5, the culture medium was changed every day. Cells were cultured at 37 °C, 5 % CO_2 in a humidified atmosphere.

Dopaminergic neuronal differentiation

The protocol for the differentiation was based on the floor-plate-based neural induction protocol reported by Kriks and colleagues (Kriks et al., 2011), with some minor variations as detailed in (Castelo Rueda et al., 2023; Zanon et al., 2017). Human iPSC colonies were disaggregated into single cells using accutase and replated onto matrigel (BD)-coated dishes in mTeSR™ 1 complete medium, supplemented with 10 µM ROCK inhibitor Y-27632 (Miltenyi Biotech). Differentiations were started with a seeding density of 40,000 cells/cm^2 for the 3x*SNCA* line and 50,000 cells/cm^2 for the CTRL line by adding knockout serum replacement (KSR, Gibco) medium supplemented with SMAD pathway inhibitors SB431542 (SB, Miltenyi Biotech) and LDN-193189 (LDN, StemMACS). On days 1 to 5, KSR medium was added to the cells in the presence of SB, LDN, recombinant Human Sonic Hedgehog (SHH, R&D System), recombinant Human FGF-8a (FGF8, R&D System), and Purmorphamine (Pu, StemMACS). The Wnt pathway activator molecule CHIR99021 (CH, StemMACS) was included from days 3-12. During days 6-10 of differentiation, increasing amounts of Neurobasal medium plus B27 supplement (NB-B27 medium, Thermo Fisher Scientific) was added to the KSR medium (25%, 50%, 75%), and upon day 7, SHH, FGF8 and Pu were withdrawn. On day 11, maturation of dopaminergic neurons was initiated by adding recombinant Human BDNF (Peprotech), ascorbic acid (Sigma Aldrich), recombinant Human TGF-ß3 (Peprotech), cyclic-AMP (EnzoLifescience) and DAPT (Tocris). Cells were passaged between

days 12 and 15 *en bloc*, and between days 20 and 25 of differentiation they were replated as single cells onto plastic dishes, previously coated with poly-D-lysine (Sigma Aldrich) and laminin (Sigma Aldrich) and collected at day 60 of differentiation to evaluate gene expression and protein levels. For oxygen consumption rate assay experiments, neurons were replated at day 30 on 96 well plates (Perkin Elmer), where they were stabilized and further differentiated until day 35. The experimental procedure is outlined in Supplementary Material Section S1.1.

Treatment conditions for SH-SY5Y cells and dopaminergic neurons

Cells were treated with 5 µM ferric chloride (Sigma-Aldrich, 10025-77-1), 50 µM dopamine (Sigma-Aldrich, H8502), and dopamine in combination with ferric chloride at the same concentrations, 5 µM deferoxamine (DFO) (Sigma-Aldrich, 2604), or DFO in combination with dopamine, for 16 hours. To prevent endogenous dopamine degradation, 100 nM tranylcypromine (Calbiochem, 3980) was added to all treatment conditions.

RNA extraction and quantitative real-time PCR (qRT-PCR)

Cells were lysed with TRIzol® Reagent (Thermo Fisher Scientific, 15596026), and RNA was extracted with the phenol-chloroform-based procedure or using Direct-zol RNA Miniprep Plus kit (Zymo research, R2070) following the manufacturer's protocols. RNA was reverse transcribed using SuperScript VILO cDNA Synthesis Kit (Thermo Fisher Scientific, 11756050) and diluted to an RNA-corresponding concentration of 5 ng/µl. qRT-PCR was performed with 10 ng of cDNA on the CFX96 Real-Time PCR Detection System (Bio-Rad) either with the SsoAdvanced™ Universal Probes Supermix (Bio-Rad, 1725284) or SsoFast™ EvaGreen® Supermix (Bio-Rad, 1725200). Gene expression was calculated with the ΔΔCt method in the CFX96 Manager software (Bio-Rad).

High-resolution respirometry (HRR) in neuroblastoma SH-SY5Y cells

High-resolution respirometry experiments were performed at 37 °C with continuous stirring (750 rpm) using the Oxygraph-2k (O2k, Oroboros Instruments, Innsbruck, Austria) as previously described (Castelo Rueda et al., 2023) with minor changes. After 16 hours of treatments, $1x10^6$ SH-SY5Y cells were resuspended in mitochondrial respiration medium MiR05 (Oroboros MiR05-Kit, Innsbruck, Austria). Oxygen consumption of permeabilized cells was measured applying the substrate-uncoupler-inhibitor titration protocol *SUIT-008 O2 ce-pce D025* (Lemieux et al., 2017). After measuring ROUTINE respiration, cells were permeabilized with optimum digitonin concentration (10 µg/ml (Doerrier et al., 2018)). Afterwards, NADH-linked substrates pyruvate (5 mM) and malate (2 mM) were added to evaluate the non-phosphorylating resting state LEAK state (PM_L), followed by the addition of kinetically saturating concentration of ADP (2.5 mM) to assess OXPHOS capacity P (PM_P). Cytochrome *c* (10 µM) was used to test the integrity of mitochondrial outer membrane (PMc_P). Glutamate (10 mM) was injected as an additional substrate for the NADH-pathway (PGM_P). Next, succinate was added to reconstitute convergent respiration through the NADH&succinate-pathway ($PGMS_P$). Uncoupler titration (0.5 µM) of the protonophore carbonyl cyanide-p-trifluoromethoxy

phenyl hydrazone, FCCP) was performed to obtain the electron transfer (ET) capacity *E* (noncoupled ET-state, $PGMS_E$) and maximal respiration. Finally, residual oxygen consumption was evaluated after inhibiting Complex I and Complex III with rotenone (0.5 µM) and antimycin A (2.5 µM), respectively. We finally calculated the flux control ratio (*FCR*) by dividing the oxygen flow measurements acquired during the individual respiratory states by the one acquired in $PGMS_E$ state.

For living cells, $1x10^6$ SH-SY5Y cells cultured in DMEM/F12+GlutaMAX™ supplement were resuspended in mitochondrial respiration medium MiR05 (Oroboros MiR05-Kit, Innsbruck, Austria). Oxygen consumption of living cells was measured by applying the substrate-uncoupler-inhibitor titration protocol *SUIT-003 O2 ce-pce D020* (Doerrier et al., 2018). After measuring ROUTINE respiration and verifying cell membrane integrity by adding pyruvate (5 mM), oligomycin (5 nM) was added to block the ATP synthase to reach the non-phosphorylating resting state (LEAK state, *L*(Omy)). Afterwards, we proceeded with uncoupler titrations of FCCP (0.1 µM steps) to obtain maximum electron transfer (ET) (noncoupled ET-state, *E*) measurements. Next, we blocked Complex I with rotenone (0.5 µM) and evaluated cell viability upon succinate titration (10 mM). At the end, we assessed the residual oxygen consumption (*Rox*) in the ROX state by antimycin A titration (2.5 µM).

Respirometric measurements and data analysis were performed using the software DatLab 7.4 (Oroboros Instruments, Innsbruck, Austria). All reagents were purchased from Sigma-Aldrich. After the O2k run, cell suspensions were collected, snap-frozen, and stored at -80 ˚C to perform citrate synthase activity measurement.

Oxygen consumption rate in hiPSC-derived neurons

Measurement of the oxygen consumption rate (OCR) in hiPSC-derived neurons was performed with a fluorescence-based Extracellular O_2 Consumption Assay Kit (Abcam, ab197243) as described previously (Castelo Rueda et al., 2023). 200,000 cells/well were seeded on 96-well plates, and the medium was replaced with 150 µl of fresh NB-B27 medium for ROUTINE OCR measurements, or with 150 µl of NB-B27 medium containing 2.5 µM FCCP for maximal respiration (ET capacity) measurements. Next, 10 µL of Extracellular O_2 consumption reagent were added to each well, except to the blank control, and 100 µl of high-sensitivity mineral oil (pre-heated at 37°C) were added to limit back diffusion of ambient oxygen. Fluorescence intensities were measured using the EnVision 2105 Multimode Plate Reader (Perkin Elmer), pre-heated at 37°C, in 2-min- intervals for a total of 200 min, at excitation/emission wavelengths = 355/642 nm. Respiration of cells results in oxygen depletion from the surrounding environment, causing an increase of fluorescence signal. Immediately after performing the OCR assay, the CyQuant™ proliferation assay (Thermo Fisher Scientific, C35012) was employed to determine the number of live cells in each well, according to the manufacturer´s instructions. Fluorescence intensity was corrected with the blank control, and OCR was determined by selecting the linear portion of the signal profile and applying the linear regression to

determine the slope. OCR calculated for each well was normalized to the cell number. OCR fluorescence intensities are expressed as relative fluorescence units (RFU) versus time (min).

Mitochondrial DNA copy number

Genomic DNA was extracted with QIAamp DNA Blood Mini Kit (Qiagen, 51104) and quantified with NanoDrop 1000 (Thermo Fisher Scientific). 5 ng of DNA were used for evaluating the quantity of mitochondrial *MT-ND1* (VIC) and nuclear *B2M* (FAM) genes by qRT-PCR using TaqMan™ Gene Expression Assays (Thermo Fisher Scientific) with Taqman probes as described in (Wasner et al. 2022). Each sample was run in triplicate, and gene expression was calculated with the following formula: mtDNA copy number (CN)=2x[$2^{(ct\ B2M-ct\ ND1)}$].

Citrate synthase (CS) activity assay

Snap-frozen cell suspensions from O2k experiments were used for citrate synthase (CS) activity measurements, which were performed following the approach described in (Castelo Rueda et al., 2023), where the final concentrations for the reaction were acetyl-CoA 100 µM, oxalacetate 100 µM and 5,5'-dithiobis- (2-dinitrobenzoic acid) 100 µM in tris chloride buffer, pH 8 (100 mM). CS was assayed spectrophotometrically at 412 nm and 30°C on an EnVision Multimode Plate Reader (Perkin Elmer). All measurements were run in duplicate for each high resolution respirometry experiment, together with a blank control.

Aconitase activity assay

Aconitase activity was measured with Aconitase Activity Assay Kit (Sigma-Aldrich, MAK051) according to manufacturer's instructions. Briefly, $1.5x10^6$ cells were used for cell fractionation, and cytosolic as well as mitochondrial aconitase enzyme activities were measured as colorimetric signal in a coupled enzyme reaction. Absorbance was measured at 450 nm with the EnVision Multimode Plate Reader (Perkin-Elmer).

Flow cytometry

Cells were stained for 15 min with 2.5 µM MitoSOX Red (Thermo Fisher Scientific, M36008) or for 30 min with 5 µM CellROX™ Green Flow Cytometry Assay Solution (Thermo Fisher Scientific, C10492) in fresh DMEM/F12+Glutamax w/o FBS and P/S. Cells were resuspended in 150 µl of FACS buffer (PBS supplemented with 0.5 % fetal bovine serum and 2 mM EDTA) containing DAPI (1:50,000, Sigma-Aldrich) as previously described (Fischer et al. 2021). Data were acquired using a CytoFLEX S flow cytometer (Beckman Coulter) and analyzed with FlowJo software (version 10.6.1, FlowJo LLC).

Protein extraction and Western blotting

Western blot was performed as described previously (Castelo Rueda et al., 2023; Fischer et al., 2021). Harvested cells were resuspended in cold RIPA buffer (Thermo Fisher Scientific) supplemented with protease inhibitors complete™ Protease Inhibitor Cocktail (Roche) and phosphatase inhibitors PhosSTOP EASYpack phosphatase inhibitors (Roche). Protein concentrations were assessed using BCA Protein Assay Kit (Thermo

Fisher Scientific), and 10 µg of total protein lysates were loaded per well on a NuPAGE 4-12% Bis-Tris SDS-PAGE gel (Thermo Fisher Scientific). The following antibodies were diluted in 1 % non-fat dry milk in TBS-T: mouse anti-TFR1 antibody (1:1,000, Thermo Fisher Scientific, 13-6800, RRID:AB_2533029), rabbit anti-FPN antibody (1:2,000, Eurogentec, NRU 451443), rabbit anti-FTH (1:500, Sigma-Aldrich, F5012, RRID:AB_259622); rabbit anti-ACO2 (1:1,000, Abcam, ab129069, RRID:AB_11144142); rabbit anti-MFRN2 antibody (1:1,000, Bioss antibodies, bs-7157R), rabbit anti-FTMT antibody (1:1,000, Abcam, ab93428, RRID:AB_1056471), mouse anti-Nitrotyrosine antibody (1:1,000, Abcam, ab7048, RRID:AB_305725), mouse anti-GAPDH (1:10,000, Millipore, MAB374, RRID:AB_2107445), rabbit anti-PGC-1α (H300) (1:1,000, Santa Cruz Biotechnology, sc-13067, RRID:AB_2166218), rabbit anti-SOD2 (1:1,000, Cell Signaling Technology, 13141, RRID:AB_2636921), rabbit anti-β-actin (1:1,000; Sigma-Aldrich, A2066, RRID:AB_476693). Appropriate horseradish peroxidase (HRP)-conjugated secondary antibodies (1:2,000, Agilent Dako, P0448 polyclonal goat anti-rabbit immunoglobulins, RRID:AB_2617138; 1:4,000, Agilent Dako, P0447 polyclonal goat anti-mouse immunoglobulins, RRID:AB_2617137) were incubated in 1 % non-fat dry milk in TBS-T. The chemiluminescence signal was detected using the ChemiDoc™ Touch Imaging System (BioRad) and quantified by densitometry using Image Lab 6.0 analyzer software (BioRad). Optical density values assessed for target proteins were normalized by the indicated loading control.

Atomic absorption spectroscopy (AAS)

Intracellular iron content was measured by AAS as described previously (Theurl et al., 2016) using the Solaar M6 Dual Zeeman spectrometer (Thermo Scientific) with continuum source (QuadLine) and Zeeman background correction system.

Extraction of intracellular metabolites

Metabolites were extracted as described previously (Gomez-Giro et al., 2019; Jager et al., 2016) with some minor modifications. Briefly, hiPSC-derived neuronal cell pellets were thawed on ice, and metabolites were extracted with water/methanol/chloroform, obtaining a three-phase system, where polar metabolites were enriched in the upper phase, non-polar metabolites in the lower phase, and cell debris constituted a solid interphase. The extraction fluid containing methanol (MeOH) and MilliQ H_2O (4:1, v/v) was supplemented with seven internal standards (IS) (see Supplementary Material Section S1.1). Cells were homogenized with the extraction fluid, and then, the liquid-liquid extraction was performed by sequentially adding water/methanol/chloroform. The upper and lower phases were divided into separate tubes for the analysis of polar and non-polar metabolites and were evaporated to dryness using a Labconco CentriVap centrifugal vacuum concentrator at -4 °C overnight. Then, polar extracts were reconstituted in acetonitrile:MilliQ H_2O (80:20, v/v), filtered with 0.2 µm PHENEX-RC 4 mm syringe filters, and transferred to Liquid Chromatography (LC)-vials, while non-polar extracts were reconstituted in toluene:methanol (1:9, v/v), centrifuged and transferred to LC-vials. Further details are given in the Supplementary Material Section S1.2 and Table S1.

Liquid chromatography-high resolution mass spectrometry analysis

LC-high-resolution mass spectrometry (LC-HRMS) was carried out on a Thermo Scientific Vanquish Flex Quaternary LC coupled to a Thermo Q Exactive HF mass spectrometer. Two separate chromatographic runs were performed: hydrophilic interaction liquid chromatography (HILIC), for polar extracts, using the method reported in (Talavera Andujar et al., 2022) and reversed phase (RP), for non-polar extracts, adapting the method reported in (Cajka et al., 2017). Further details are given in the Supplementary Material, Section S1.3.

Metabolomics data processing and analysis

Data processing was conducted using MS-DIAL (version 4.9.221218) (Tsugawa et al., 2020) as previously described (Talavera Andujar et al., 2022). For the analysis of polar fractions, the following libraries provided by MS-DIAL were used: MSMS_Public_EXP_Pos_VS17 and MSMS_Public_EXP_NEG_VS17 (16,481 unique compounds for MS/MS positive and 9,033 unique compounds for negative, respectively). Tentative identifications obtained from MS/MS spectral matching in MS-DIAL were compared against the retention times (RT), exact masses, and MS/MS of authenticated standards (**Table S1**) measured using the same method to obtain Level 1 confidence (i.e., confirmed structure) (Schymanski et al., 2014). Those features that were not present in the library were analyzed in MetFrag (Ruttkies et al., 2016) using the PubChemLite chemical database (31 March 2023 1.20.0 version) (Bolton et al., 2023; Schymanski et al., 2021) for tentative identification using *in silico* fragmentation.

For non-polar fractions, "lipidomics" was chosen as target omics in MS-DIAL, and an internal *in silico* database of MS-DIAL was used for tentative identification. Only features with MS/MS spectral matches with the MSP databases were considered for further analysis. Peaks were manually checked and additionally run in MetFrag for tentative identification using *in silico* fragmentation. Lipids satisfying these checks were classified with a confidence level 3a and were included for studying differences between the two cell lines and/or impact of iron and dopamine treatments. Criteria for confidence levels are reported in **Table S2**.

Statistical analyses

Statistical analyses were performed with GraphPad Prism 9. When comparing treatments within one group, one-way ANOVA was used followed by Dunnett's test to correct for multiple comparisons. For analyzing differences after treatments between groups in hiPSC-derived neurons, two-way ANOVA was used followed by Šídák's test to correct for multiple comparisons. Mann Whitney test or a parametric unpaired t-test was used to compare differences between two groups. For the metabolite analyses, peak areas were normalized by sum of the total intensity (TIC). Statistical significance was tested using parametric unpaired t-test with Welch's correction to assess metabolic differences between the control and the diseased cell lines (CTRL vs. 3x*SNCA*). For metabolites with different amounts between the two cell lines, a two-way ANOVA Šídák's multiple comparisons test was performed to evaluate if iron or dopamine treatments had an impact on metabolite levels.

Results

Dopamine affects iron metabolism in SH-SY5Y cells

To investigate the effect of dopamine on cellular iron homeostasis in neuroblastoma SH-SY5Y cells, we examined the expression of critical cellular iron metabolism genes, including transferrin receptor 1 (*TFRC*, *TFR1*) and ferroportin (*SLC40A1*, *FPN*), which reflect the major avenues for cellular iron uptake and release, respectively (David et al., 2022; Muckenthaler et al., 2017), ferritin (FTH), the principal cellular iron storage protein consisting of heavy (FTH) and light chain subunits, as well as mitoferrin2 (*SLC25A28*, *MFRN2*), an iron transporter into mitochondria and good indicator of mitochondrial iron status (Ali et al., 2022; Muhlenhoff et al., 2015). Cells were treated with iron ($FeCl_3$) or the iron chelator DFO for testing cellular responses to iron supplementation or depletion, and with dopamine alone or in combination with both compounds for analyzing their interaction. For iron and dopamine, different concentrations were tested. Based on our previous work (Dichtl et al., 2018), we screened for effects on *TFR1* mRNA expression and cellular toxicity after 16 hours of incubation. As a result, we selected 50 µM dopamine and 5 µM iron because higher iron concentrations resulted in cellular toxicity in this cell line, specifically when combined with dopamine (**Figure S1**). DFO showed anticipated effects on the regulation of iron genes, whereas iron, which was used at lower dosages as in other cellular systems and published reports (Dichtl et al., 2018), caused only small effects. Tranylcypromine was added to all treatments to prevent endogenous dopamine degradation, and an untreated condition was included to evaluate the basal expression of the investigated genes (Dichtl et al., 2019; Dichtl et al., 2018; Mercuri et al., 2000).

As expected, DFO treatment significantly increased *TFR1* mRNA expression (p=0.001) indicating effective chelation of cellular iron. However, DFO did not affect *FPN* mRNA expression. Interestingly, dopamine upregulated both *TFR1* (p=0.043) and *FPN* (p=0.011) mRNA levels (**Figure 1A**). In addition to *TFR1*, we investigated the expression of *DMT1* (divalent metal transporter 1), another protein involved in cellular iron uptake, which followed the trend of *TFR1* upon dopamine treatment (**Figure 1A**). Regarding mitochondrial iron status, dopamine significantly upregulated *MFRN2* (p=0.042) (**Figure 1A**). To exclude unspecific effects of dopamine, $FeCl_3$, and DFO or combinations thereof, we analyzed cellular viability, which was affected only by the combined treatment of DFO with dopamine (**Figure S2**). We also tested differentiation of SH-SY5Y cells with retinoic acid and cholesterol (Cheung et al., 2009; Teppola et al., 2016) and verified the expression of genes of interest, which did not result in major differences between differentiated and undifferentiated cells (**Figure S3A**).

To investigate whether the observed effects on iron metabolism-related gene expression translated into corresponding changes of protein expression, we quantified protein levels by means of western blotting. Dopamine treatment resulted in increased TFR1 protein levels (p=0.029), in a similar way as DFO treatment (p=0.012) and their combination (p=0.032), further suggesting that dopamine supplementation may result in promotion of iron uptake possibly as a consequence of iron binding by dopamine (Dichtl et al., 2018) (**Figure**

1B, C; Figure S3B). Of note, no significant changes of FTH expression were observed upon dopamine supplementation, while for FPN no dopamine-induced upregulation on the protein level was observed (**Figure 1B, C; Figure S3C**).

In addition, we evaluated protein expression of mitochondrial aconitase (mitochondrial, m-aconitase, ACO2), an iron-sulfur (FeS) cluster containing enzyme that catalyzes the interconversion of citrate to iso-citrate as part of the tricarboxylic acid (TCA) cycle (Beinert and Kennedy, 1993), and because its translation is controlled by cellular iron availability (Muckenthaler et al., 2017). As an indicator of oxidative and nitrosative stress responses in the cell, we also determined nitrotyrosine (3-NT) (Kuhn et al., 2004). Protein levels of ACO2 were found to be significantly decreased upon dopamine ($p= 0.029$) treatment, which would be in line with translational repression by iron deficiency as described previously (Oexle et al., 1999). Of note, dopamine treatment resulted in higher 3-NT levels, indicative for intracellular oxidative stress, which can also impair ACO2 expression (Liang and Patel, 2004) (**Figure 1B, C; Figure S3B**).

Since the data on gene and protein expression suggest alterations in cellular iron status after dopamine treatment, intracellular iron levels were measured by AAS. Dopamine treatment was associated with a significant increase of total intracellular iron levels ($p=0.032$). $FeCl_3$ and DFO treatments resulted in a trend for increased and decreased intracellular iron measurements, respectively, as expected (**Figure 1D**).

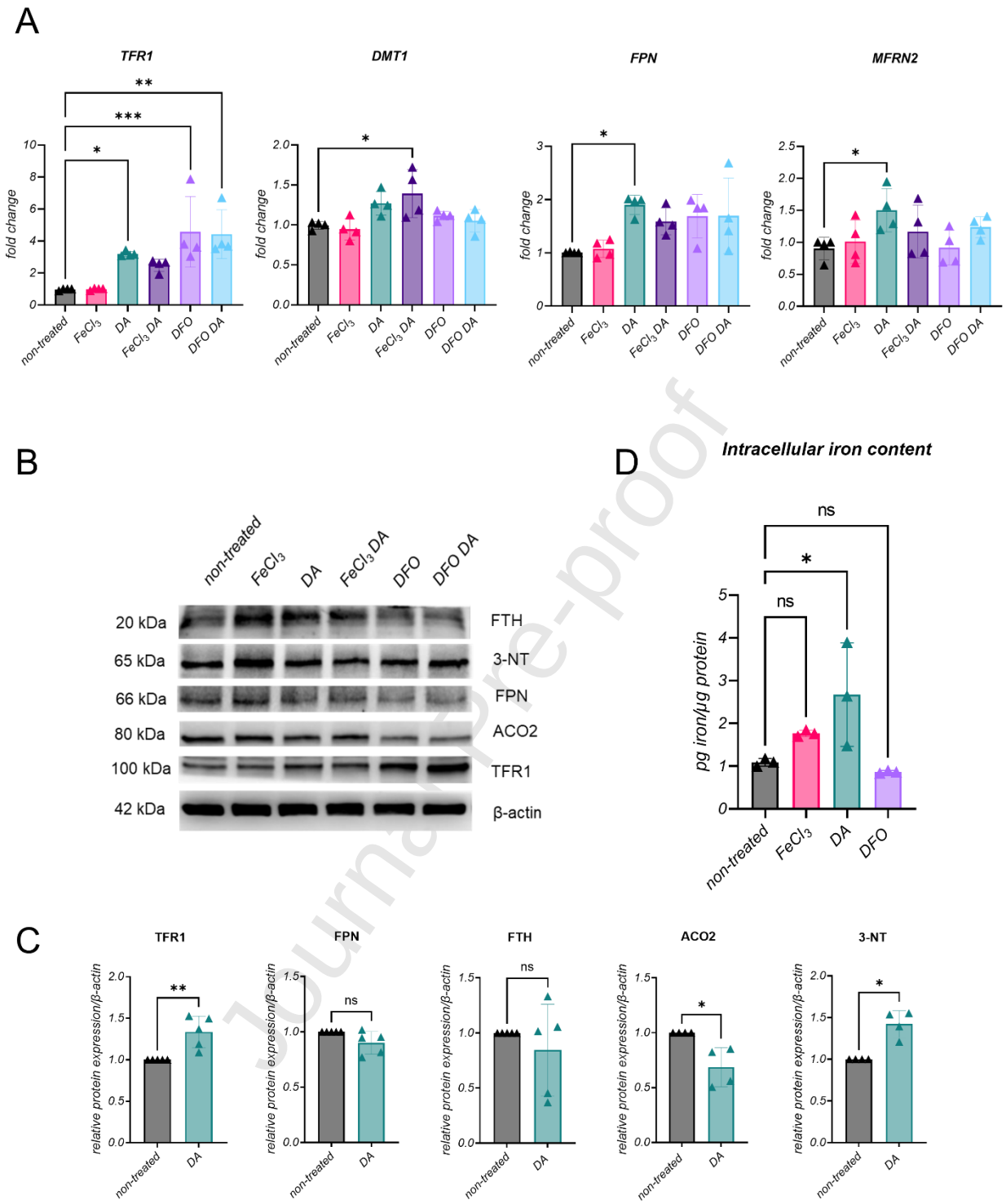

Figure 1. Expression levels of genes and proteins involved in iron metabolism and intracellular iron levels in SH-SY5Y cells. *A) TFR1, DMT1, FPN, and MFRN2 mRNA expression levels normalized with TUBA1A (tubulin); n=4. B) Representative western blot showing TFR1, FPN, FTH, ACO2, 3-NT protein levels upon treatments; β-actin was used as a loading control. Molecular mass markers are in kilodaltons (kDa). C) Densitometric analyses of TFR1, FPN, FTH, ACO2 and 3-NT protein levels after treatment with dopamine, normalized to the loading control β-actin and to the non-treated condition; n≥3. Statistical differences were calculated by Mann Whitney test. *p≤0.05. D) Intracellular iron levels measured by atomic absorption spectroscopy in cells treated with dopamine, iron and DFO. Results were normalized to protein content; n=3. Statistical differences were calculated by ordinary one-way ANOVA followed by Dunnett's test to correct for multiple testing. *p≤0.05; **p≤0.01; ***p≤0.001.*

Dopamine affects mitochondrial fitness in SH-SY5Y cells

Since the data collected thus far indicated that dopamine treatment of SH-SY5Y cells altered cellular iron homeostasis, ACO2 protein levels and oxidative stress response, we questioned whether dopamine directly affects mitochondrial function. We measured mitochondrial respiration by HRR in living and permeabilized SH-SY5Y cells upon treatment with dopamine, $FeCl_3$ and the combination of both compounds, because iron is necessary for mitochondrial function (Volani et al., 2017). Representative traces of real-time oxygen consumption illustrate the multiple substrate-uncoupler-inhibitor titration (SUIT) protocol in permeabilized SH-SY5Y cells (**Figure 2A**).

In living (non-permeabilized) cells, differences upon dopamine treatment were evident in the maximal respiration (ET), indicating a noncoupled respiration (**Figure S4**). In permeabilized cells treated with dopamine or $FeCl_3$ combined with dopamine, we observed a decreased oxygen consumption after titration of kinetically saturating concentrations of ADP in the presence of pyruvate and malate (PM_P) (p=0.023 and p=0.033, respectively), and succinate ($PGMS_P$) (p=0.033 and p=0.034, respectively). In addition, cells treated with dopamine alone showed a significant decrease in maximal oxygen flux ($PGMS_E$) (p=0.036) (**Figure 2B**).

Given the observed decrease in OXPHOS and ET capacities, we calculated flux control ratios (*FCR*) to investigate whether mitochondrial quality defects were induced by treatments. After cytochrome *c* titration, *FCR* was significantly increased by dopamine (p=0.026) and its combination with $FeCl_3$ (p=0.045) ($FCR_{(PMcP)}$). This increase was kept after glutamate addition (data not shown). Additionally, the treatments also increased cytochrome *c* control efficiency (*c* control efficiency) suggesting an alteration of the integrity of the mitochondrial outer membrane (dopamine: p=0.010, dopamine and $FeCl_3$: p=0.013) (**Figure 2C**). These observations suggest that dopamine and $FeCl_3$ combined with dopamine treatments change mitochondrial quantity, which may explain the observed decrease in mitochondrial respiration. On the other hand, the increase in *FCR* for NADH-pathway might indicate a compensatory mechanism.

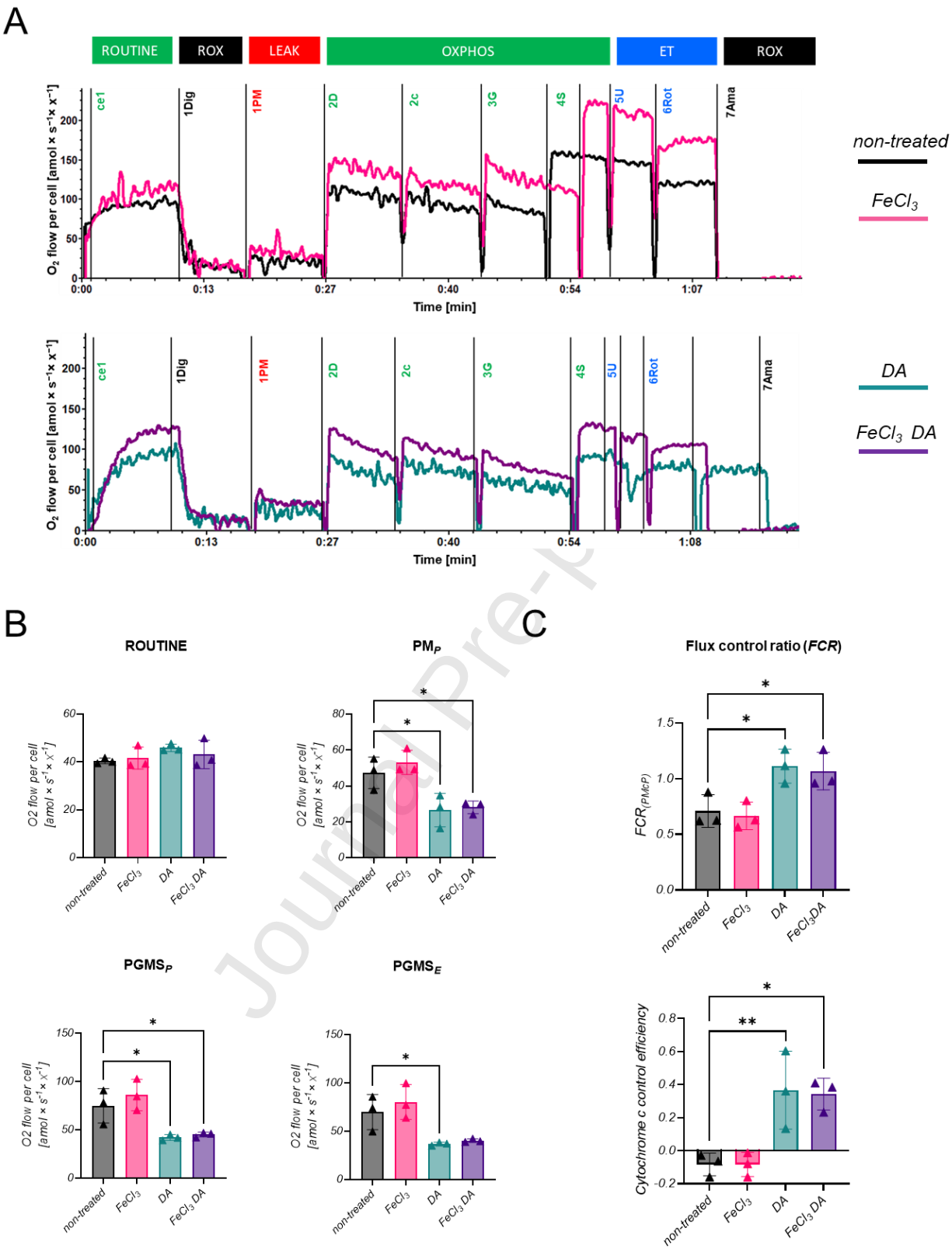

Figure 2. Effect of dopamine and $FeCl_3$ on mitochondrial respiration in permeabilized SH-SY5Y neuroblastoma cells. *A) Representative traces of oxygen consumption in permeabilized SH-SY5Y cells treated with the compounds of interest for 16 hours with sequential titrations. Respiration values were expressed as O_2 flow per cell [amol × s^{-1} × x^{-1}]; y-axis) as a function of time (x-axis). Sequential steps: addition of cells (ce1), digitonin (1Dig, 10 µg/ml), pyruvate&malate (1PM, 5 mM&2 mM), ADP (2D, 2.5*

*mM), cytochrome c (2c, 10 µM), glutamate (3G, 10 mM), succinate (4S, 10 mM), FCCP (5U, 0. 5 µM step), rotenone (6Rot, 0.5 µM), antimycin A (7Ama, 2.5 µM). Non-treated: black; $FeCl_3$: pink; DA: turquoise; $FeCl_3$ and DA: purple. B) Oxygen consumption in permeabilized SH-SY5Y cells treated with the compounds of interest for 16 hours. ROUTINE: ROUTINE respiration in the physiological coupling state controlled by cellular energy demand, energy turnover and the degree of coupling to phosphorylation; PM_P: OXPHOS capacity with PM as NADH-linked substrates; $PGMS_P$: OXPHOS capacity of the convergent NADH&succinate-pathway into Q; $PGMS_E$: noncoupled ET-state of the NADH&succinate-pathway. Each condition was measured in three independent assays. C) Flux control ratio after cytochrome c titration ($FCR_{(PMcP)}$) and cytochrome c control efficiency calculated as 1-PM_P/PMcP. Statistical analysis was carried out by using the ordinary one-way ANOVA followed by Dunnett's test to correct for multiple testing. *p≤0.05, **p≤0.01.*

Dopamine affects mitochondrial numbers and induces oxidative stress in SH-SY5Y cells

To further investigate mitochondrial homeostasis, we measured mitochondrial DNA (mtDNA) copy numbers in SH-SY5Y cells treated for 16 hours with $FeCl_3$, dopamine, and the combination of $FeCl_3$ and dopamine. We detected a significant drop of mtDNA copy number upon treatment with dopamine (p=0.022) and for concomitant dopamine with $FeCl_3$ supplementation (p=0.010) (**Figure 3A**). Compared to untreated conditions, mtDNA copy number decreased by 17.97 % after $FeCl_3$ treatment, by 38.56 % after dopamine treatment, and by 44.77 % after the treatment with iron and dopamine. To confirm these data, we measured citrate synthase activity, which is a functional marker of the amount of mitochondria, and found a decrease for all treatments compared to untreated cells, comparable to observations for the mtDNA copy number ($FeCl_3$ p=0.011; DA p=0.002; $FeCl_3$+DA: p=0.014). Together, these data indicate a reduced mitochondrial content upon treatment with dopamine, independent of $FeCl_3$ supplementation (**Figure 3B**).

Next, we measured aconitase activity to investigate whether the detrimental effect of dopamine on mitochondrial respiration and content could be mediated by oxidative stress. Aconitase 1 (cytosolic, c-aconitase, ACO1) and mitochondrial ACO2 are reversibly inactivated by oxidative stress and can therefore be used as a marker for oxidative damage (Rouault, 2006). Compared to the untreated condition, a significant decrease of ACO1 activity after dopamine treatment was detected (p=0.003), and the same trend was observed when combining dopamine with $FeCl_3$ (p=0.053), while $FeCl_3$ alone did not show an effect (**Figure 3C**). For ACO2, we observed reduced protein levels upon dopamine treatment (**Figure 1C**) along with a reduction of ACO2 activity, which was not significant upon dopamine alone but upon the combined treatment of dopamine with $FeCl_3$ (**Figure S5**).

To measure total cellular ROS and mitochondrial ROS (mROS) production, cells were stained with CellROX dye, which upon oxidation by ROS exhibits a photostable green fluorescence, and MitoSox Red dye, which specifically accumulates in mitochondria in live cells and, upon oxidation by superoxide anion, emits a red fluorescence signal. While mitochondrial superoxide anion levels remained stable for up to 16 hours in untreated cells, they started to rise after 2 hours of dopamine treatment, reaching maximum levels at 4 to 6 hours, and then dropping to baseline levels. This suggests subsequent activation of antioxidant systems in the cells that protect remaining mitochondria from oxidative stress or the removal of damaged mitochondria

(**Figure 3D**). A similar trend was detected for treatments with $FeCl_3$, dopamine and $FeCl_3$, and with DFO (**Figure S6A**). Moreover, CellROX signals, measuring generalized oxidative stress, followed a very similar pattern upon the different treatments (**Figure S6B**). ROS might trigger mitochondrial damage responsible for the decrease in mitochondrial content and quality resulting in an overall reduction of mitochondrial respiration.

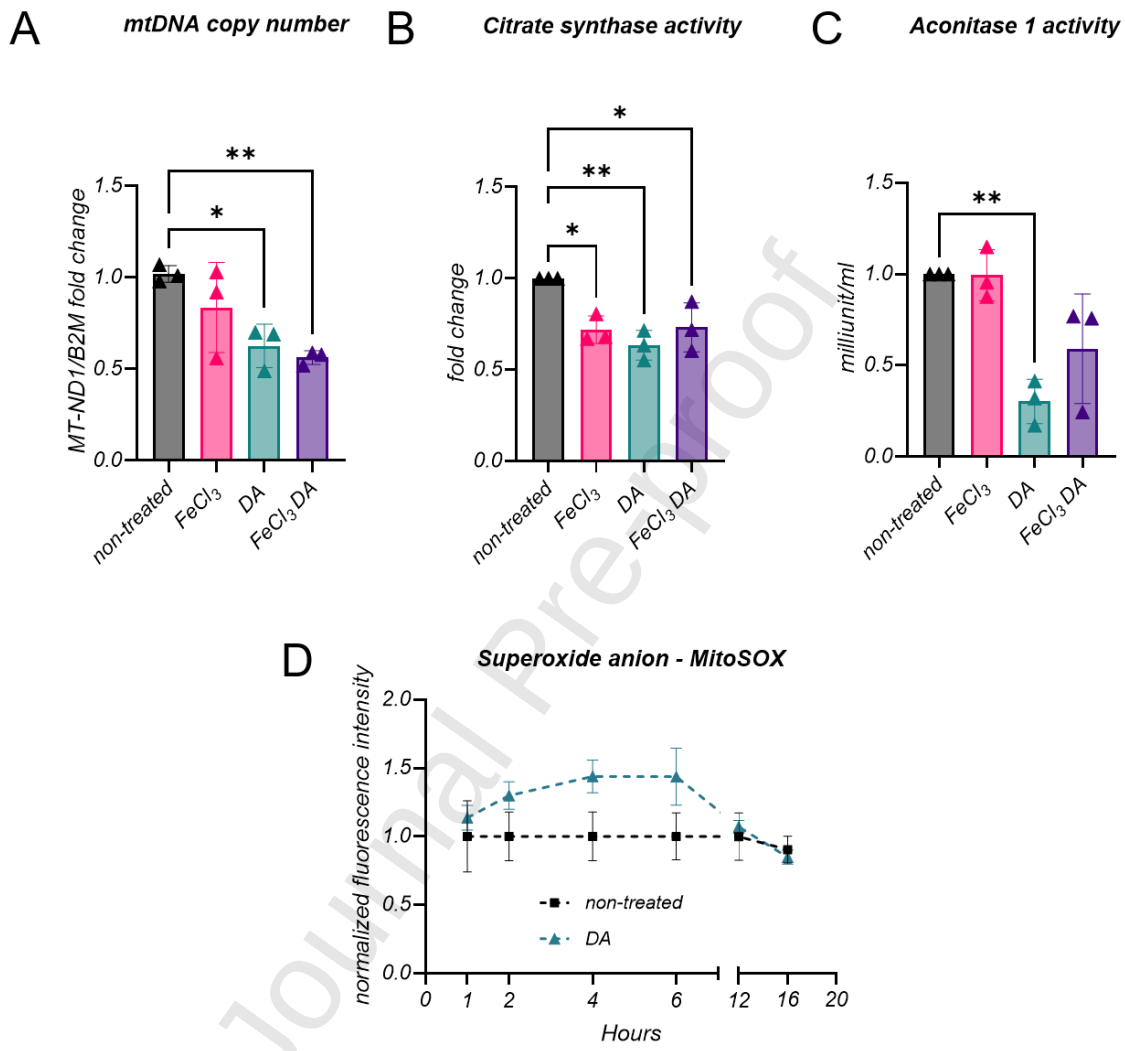

Figure 3. Evaluation of mitochondrial content and oxidative stress. *A) mtDNA copy number measured by RT-PCR of MT-ND1, normalized to B2M gene on genomic DNA of permeabilized cells after 16 hours of treatment. B) Citrate synthase activity in permeabilized cells measured after 16 hours of treatment. C) Cytosolic (c-) aconitase activity upon treatment with the compounds of interest. D) MitoSOX Red signal was quantified at different time points in non-treated conditions and upon dopamine treatment. Successively, the signal was normalized for non-treated cells. At each time point, cells treated with dopamine are compared to cells without treatment as control. Each data point represents the mean of 3 measurements ± standard deviation (SD). Statistical analysis was carried out by using the ordinary one-way ANOVA followed by Dunnett's test to correct for multiple testing. *p≤0.05; **p≤0.01.*

Dopamine affects iron metabolism in hiPSC-derived neurons

We then studied whether the effects of dopamine on SH-SY5Y cells also apply to hiPSC-derived dopaminergic neurons of a control and a PD patient-derived cell line carrying a triplication mutation of the *SNCA* gene

(3x*SNCA*). Neurons were treated for 16 hours with the compounds of interest ($FeCl_3$, DFO, dopamine or their combination) and mRNA expression of *TFR1*, *FPN,* and *MFRN2* was evaluated. Comparison of baseline mRNA expression between control and 3x*SNCA* hiPSC-derived neurons showed that *TFR1* and *FPN* were significantly increased in the PD line (p=0.0002 and p=0.005, respectively), suggesting an altered iron status in the 3x*SNCA* line, while the mitochondrial marker *MFRN2* did not differ between control and PD lines (**Figure 4A**). After dopamine treatment, there was a trend for an increased mRNA expression of *TFR1* in the control line compared to non-treated cells, which was significant in the PD line (p=0.032). *FPN* levels showed minor differences among groups in both lines. Interestingly, for *MFRN2* there were no differences upon treatments in the control line, while in the patient line, dopamine treatment significantly reduced its mRNA expression (p=0.011) (**Figure 4B**).

Since several iron transporters are regulated post transcriptionally via iron regulatory proteins and the iron-responsive element (IRE) signaling pathway (Zhou and Tan, 2017), it is important to assess their protein levels. When comparing protein levels of non-treated control and PD patient neurons, we observed that TFR1 (p=0.029) and MFRN2 (p=0.029) protein levels were higher in the 3x*SNCA* line compared to the control line. Furthermore, contrarily to the mRNA level, FPN protein expression was lower in the PD line compared to the control (**Figure 4C, D**). This again suggests that cellular iron trafficking differs in the two lines. In particular, in the patient line, alterations are suggestive of intracellular/cytoplasmic iron deficiency as reflected by higher TFR1 and lower FPN levels compared to the control line. On the other hand, higher MFRN2 and FTMT in the PD line suggests that iron is transferred to mitochondria thereby promoting mitochondrial iron accumulation. In summary, the balance between a predicted lower cytoplasmic iron content and iron accumulation in mitochondria resulted in no obvious change in total cellular iron levels as implied by the measurement of total intracellular iron content (**Figure S7**). Regarding treatments, we detected no changes of TFR1 protein levels in the control and PD lines after 16 hours of dopamine supplementation, while iron and DFO had to some extent the anticipated effects (**Figure 4**; **Figure 4G**). FPN protein levels were significantly decreased by dopamine in the control line, whereas in the patient line the low FPN levels increased with dopamine treatment (**Figure 4C; Figure 4G)**. MFRN2 levels as indicator of mitochondrial iron status remained largely unchanged by either treatment in both lines (**Figure 4G**).

When analysing peroxisome proliferator-activated receptor gamma coactivator-1α (PGC-1α), the major regulator of mitochondrial biogenesis, in the control line, dopamine decreased its protein levels (DA: p<0.0001; $FeCl_3$ DA: p<0.0001), contrarily to the PD patient line, where dopamine supplementation increased PGC-1α levels (DA: p=0.034; $FeCl_3$ DA: p=0.007) (**Figure 4C; Figure 4G).** We also measured superoxide dismutase 2 (SOD2) protein levels as an indicator of cellular stress responses. Dopamine increased SOD2 levels in both lines, but this was significant only in the PD patient neurons (p=0.039) (**Figure 4E, F**).

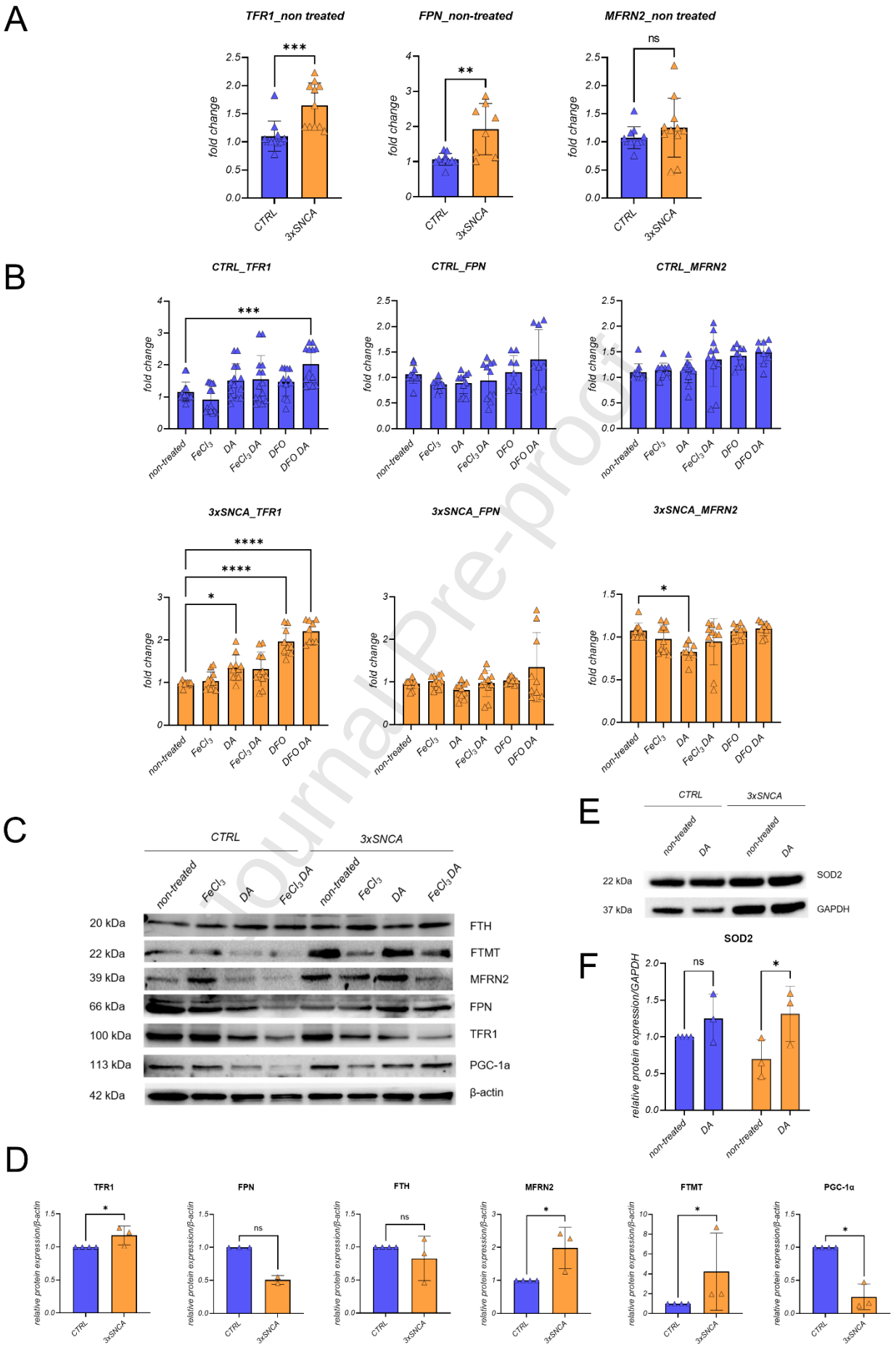

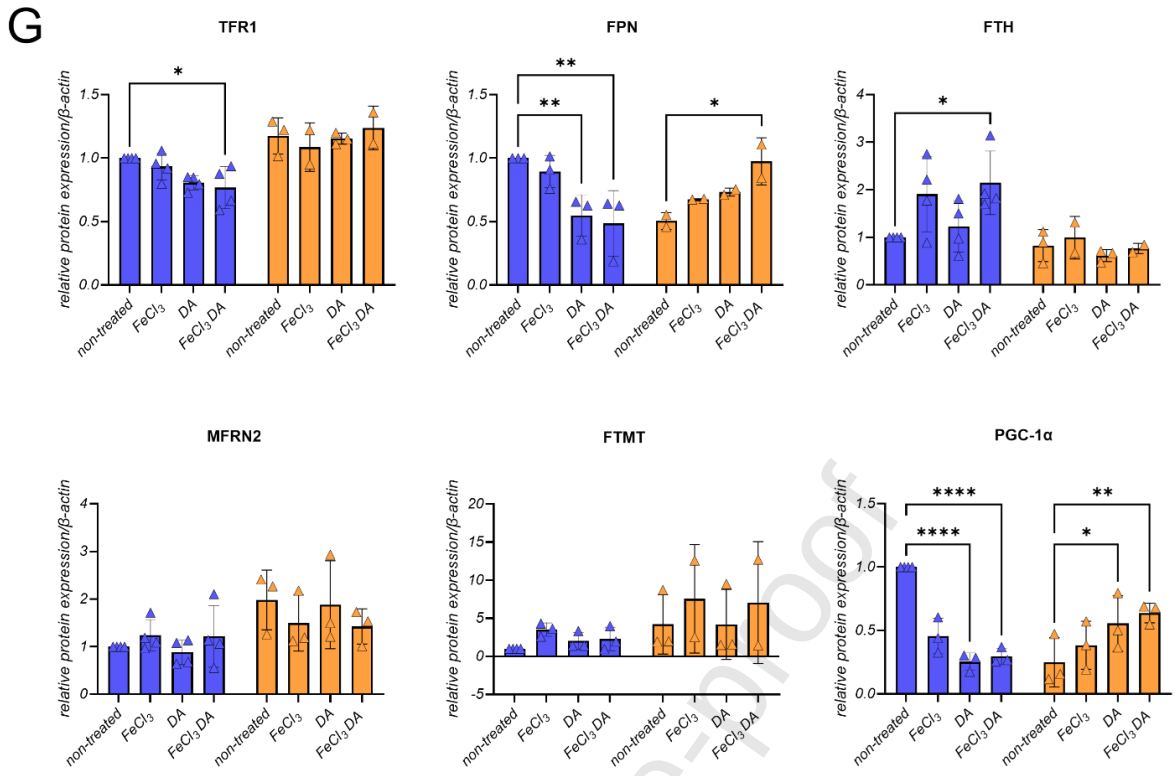

Figure 4. Expression of iron- and mitochondria- related genes and proteins in hiPSC-derived neurons. *A) Expression of TFR1, FPN, and MFRN2 normalized with tubulin in the CTRL and PD patient (3xSNCA) lines at basal conditions. B) Impact of the compounds of interest on genes involved in cellular iron metabolism and mitochondrial iron status. C) Representative western blot showing FTH, FTMT, MFRN2, FPN TFR1, PGC-1α protein expression upon treatments. Protein levels were analyzed with the indicated antibodies, and β-actin was used as a loading control. Molecular mass markers are in kilodaltons (kDa). D) Densitometric analyses of proteins found differently expressed in hiPSC-derived neurons of a CTRL and PD patient line in non-treated conditions after being resolved with WB; protein levels were normalized to the loading control and related to the CTRL line. E) Representative western blot of SOD2 protein levels upon iron and DA treatments in CTRL and mutant cells. F) Quantification of SOD2 levels in CTRL and mutant cells, normalized to the loading control GAPDH and related to the non-treated CTRL line. n≥2. G) Densitometric analyses of protein levels of crucial proteins involved in iron import and storage in cells and mitochondria, in addition to markers of mitochondrial biogenesis after treatments, normalized to the loading control β-actin and related to the non-treated CTRL line. Statistical differences were calculated by Mann Whitney test for comparisons between the two groups in untreated conditions (A, D), ordinary one-way ANOVA followed by Dunnett's test to correct for multiple testing was applied for comparison of multiple groups (B). For comparisons between non-treated and treated cells (E, G), a two-way ANOVA was performed followed by Šídák's test to correct for multiple testing. *p≤0.05, ***p≤0.001; ****p≤0.0001.*

Reduced oxygen consumption rate in hiPSC-derived patient neurons improves upon dopamine treatment

To evaluate cellular respiration in hiPSC-derived neurons (control and PD patient line) (**Figure 5A**), we quantified basal extracellular oxygen consumption rate (OCR) in ROUTINE state and after induction of maximal respiration with FCCP (ET), in both control and patient hiPSC-derived neurons with and without dopamine and $FeCl_3$ treatments (**Figure 5B**).

In non-treated conditions, the PD line showed a significantly decreased OCR in ROUTINE (p=0.008) and ET capacity (p=0.008) compared to the control line (**Figure 5C**). In the control line, dopamine treatment resulted in significantly reduced ROUTINE respiration compared to untreated cells (p=0.022), while ROUTINE respiration was not affected in the PD patient line (**Figure 5D**). After induction of maximal respiration, both $FeCl_3$ and dopamine treatments decreased OCR levels in the control line ($FeCl_3$: p=0.007; DA: p=0.025), while in the 3x*SNCA* line, dopamine treatment increased maximal respiratory capacity to control levels (p<0.0001) (**Figure 5D**).

Additionally, we calculated ET-ROUTINE control efficiency, which is an expression of the relative scope of increasing ROUTINE respiration in living cells by uncoupler titrations to obtain ET capacity, and we found a significant increase in the PD patient line upon dopamine supplementation (p=0.007) (**Figure 5E**). Reduced mitochondrial respiration in control neurons upon dopamine treatment is in line with observations made in SH-SY5Y cells, while in patient neurons dopamine induces a beneficial effect on OCR.

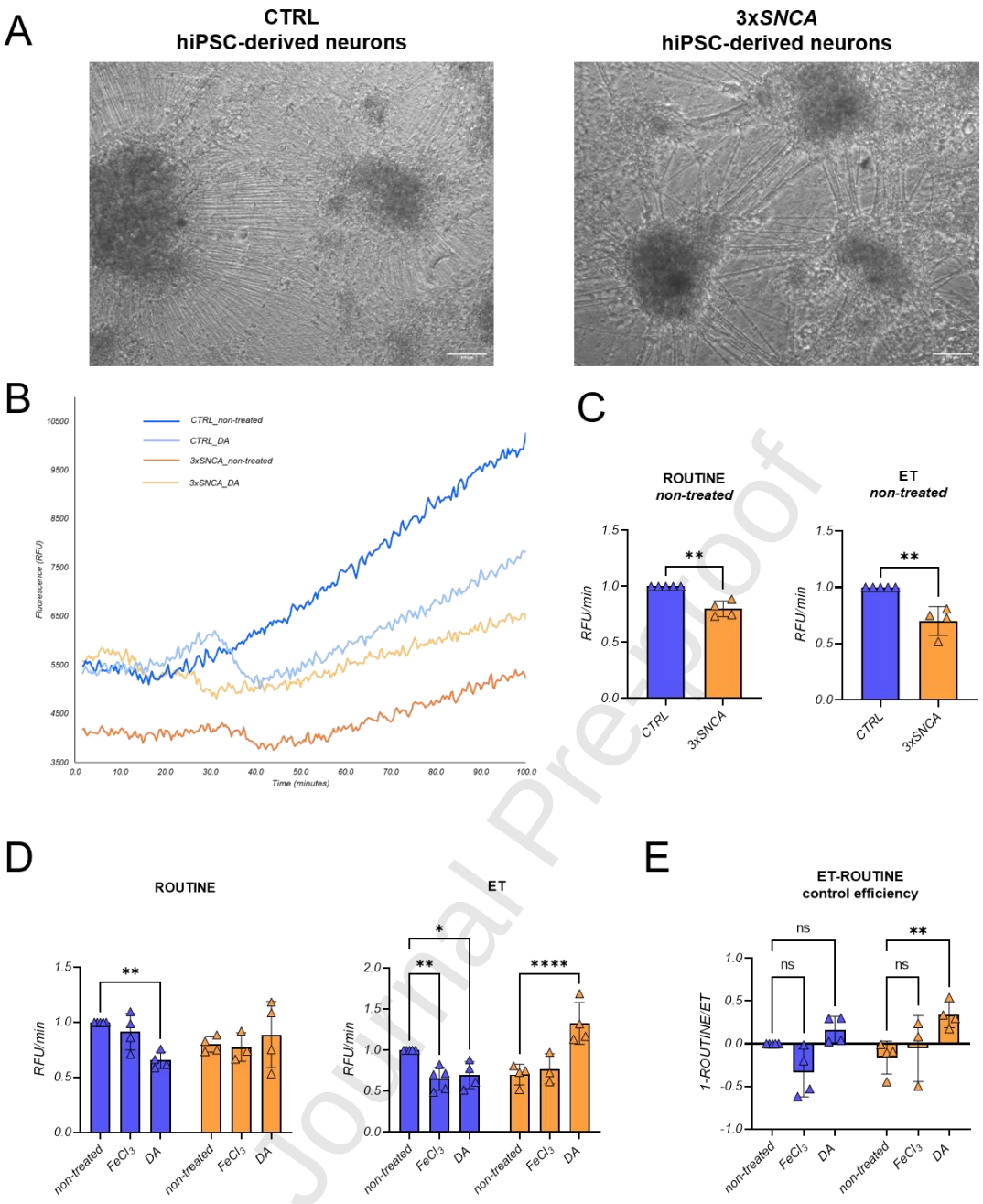

Figure 5. Oxygen consumption rates in hiPSC-derived neurons of control and PD patient line with 3xSNCA mutation. *A) Representative light microscopy images of hiPSC-derived neurons used for OCR measurement at day 34 of differentiation. Scale bar: 100 µm. B) Representative curves of the maximal respiration fluorescence signal in hiPSC-derived neurons of the non-treated control (CTRL, non-treated, blue line) versus control cells treated with dopamine (CTRL_DA, light blue line) and non-treated 3xSNCA cells (3xSNCA, non-treated, orange line) versus 3xSNCA cells treated with dopamine (3xSNCA_DA, yellow line). C) Relative quantification of ROUTINE and maximal respiration measured after the addition of 2.5 µM FCCP in the control and the PD patient lines without treatment. D) ROUTINE and maximal respiration (ET) in the control and PD patient lines after treatments with $FeCl_3$ or dopamine. E) ET-ROUTINE control efficiency calculated as 1-ROUTINE/ET in control and PD patient-derived lines after treatments with $FeCl_3$ or dopamine. n≥3 independent differentiations with 3 wells per respiratory parameter for each differentiation. Error bars represent the mean ±SD of at least 3 data points (one for each differentiation) for each experimental group.*

*p values were determined using two-way ANOVA followed by Šídák's test to correct for multiple comparisons. *p≤0.05; **p≤0.01; ***p≤0.0001; ****p≤0.00001. RFU: relative fluorescence units.*

Metabolic signature in hiPSC-derived patient neurons changes upon dopamine treatment

To better understand the metabolic changes associated with observed mitochondrial alterations between control and patient neurons, we performed an untargeted metabolomic analysis in cell pellets of neurons treated with iron or dopamine for 16 hours. Both polar and non-polar metabolites were analyzed (**Figure S8; Figure S9**). Among the identified polar metabolites confirmed with standards or putatively identified by *in silico* fragmentation, 12 were significantly different between patient and control neurons under basal conditions, while 4 metabolites showed a trend towards reduction (malic acid, methionine) or increase (inosine, citrulline) in the PD line compared to the control line. Specifically, threonine, serine, glutamic acid, glutamine, taurine, N-acetylneuramic acid, uridine 5'-monophosphate, acetylcarnitine, and creatine were significantly decreased in the PD line compared to the control, while succinic acid, propionylcarnitine, and lactate were significantly increased in the PD line (**Figure S8**). In addition, we calculated the ratio between propionylcarnitine and acetylcarnitine as additional biomarker of abnormalities in propionate catabolism as suggested by increased propionyl carnitine (Collado et al., 2020), demonstrating an increased ratio in the PD line compared to the control line (**Figure S10A**). Among the investigated metabolites, those affected most by iron or dopamine treatments were threonine, serine and glutamic acid in both lines but with opposite trends: while in the control neurons dopamine resulted in significantly reduced levels, in the PD patient neurons dopamine treatment increased the levels of these metabolites towards the concentrations found in untreated control neurons (threonine – CTRL $FeCl_3$: p=0.003; DA: p=0.005 – 3x*SNCA* DA: p=0.012; serine – CTRL DA: p=0.020 - 3x*SNCA* DA: p=0.003; glutamic acid – CTRL $FeCl_3$: p=0.032; DA: p=0.012 – 3x*SNCA* DA: p= 0.012). Furthermore, glutamine and creatine showed a non-significant trend towards increased levels after dopamine treatment in the PD patient line and reduction in the control line. Succinic acid levels were affected by dopamine only in the PD line (p=0.037) but not in the control line (**Figure 6**). Dopamine treatment also affected the ratio between propionylcarnitine and acetylcarnitine with a trend towards decreased levels in the patient line (**Figure S10B**). A list of all detected polar metabolites is reported in **Table S3**.

Serine, threonine, and creatine belong to the glycine, serine, threonine metabolism pathway, and they are all crucially involved in mitochondrial function and energy production (**Figure 7**). Their reduction in the PD neurons compared to the control neurons (**Figure S8**) further confirms impaired energy metabolism in the PD line.

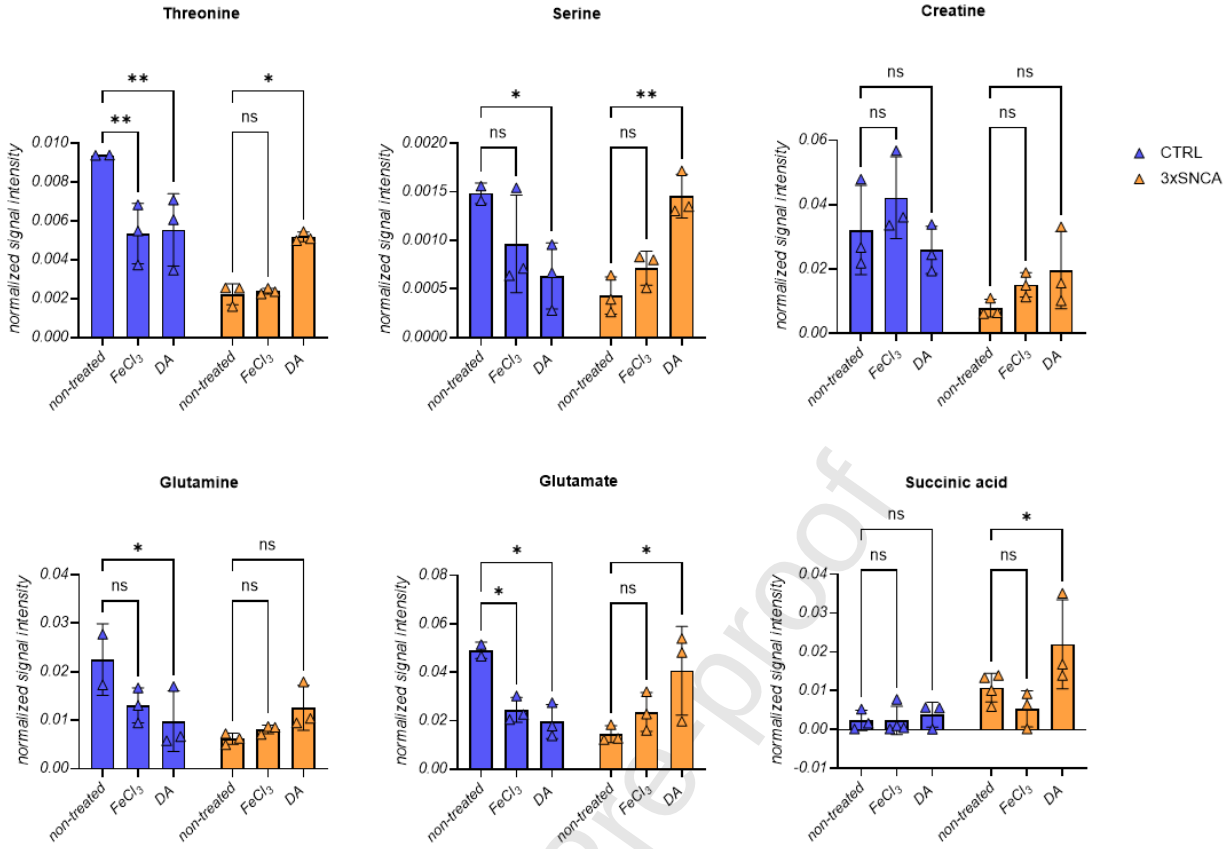

Figure 6. Polar metabolites affected by dopamine or $FeCl_3$ treatments. *Blue=Control (CTRL) line; orange=3xSNCA line. n=3 independent differentiations. Error bars represent the SD. p values were determined using a two-way ANOVA followed by Šídák's test to correct for multiple comparisons. *p≤0.05; **p≤0.01.*

Among the non-polar metabolites, 100 features were detected, of which 18 and 17 metabolites were tentatively identified at level 3 in positive and negative ionization modes, respectively (**Table S4**). Ten lipids were significantly altered in the patient hiPSC-derived neurons under basal culture conditions, including coenzyme Q10, which is a crucial electron carrier in the electron transfer system and a lipophilic antioxidant preventing the generation of free radicals, and some glycerophospholipids/sphingolipids (**Figure S10B, C**). Iron treatment did not influence these metabolites, and dopamine affected lipid levels only in the control line (i.e. PE(18:0/0:0), PC(18:1(9E)/0:0)) but not in the patient line, except for cholesterol sulfate, which was decreased upon dopamine treatment reaching levels comparable to those found in the control line (**Figure S11**). Examination of the metabolic changes by lipid class (**Figure S12A, B**) revealed that both sphingolipids and glycerophospholipids are reduced in the PD line compared to the control line, and dopamine did not affect the levels of these lipids (**Figure S12C, D**). In general, the main metabolic alterations are related to mitochondrial metabolism (**Figure 7**), and dopamine supplementation beneficially affected their dysregulated levels in PD cells.

A

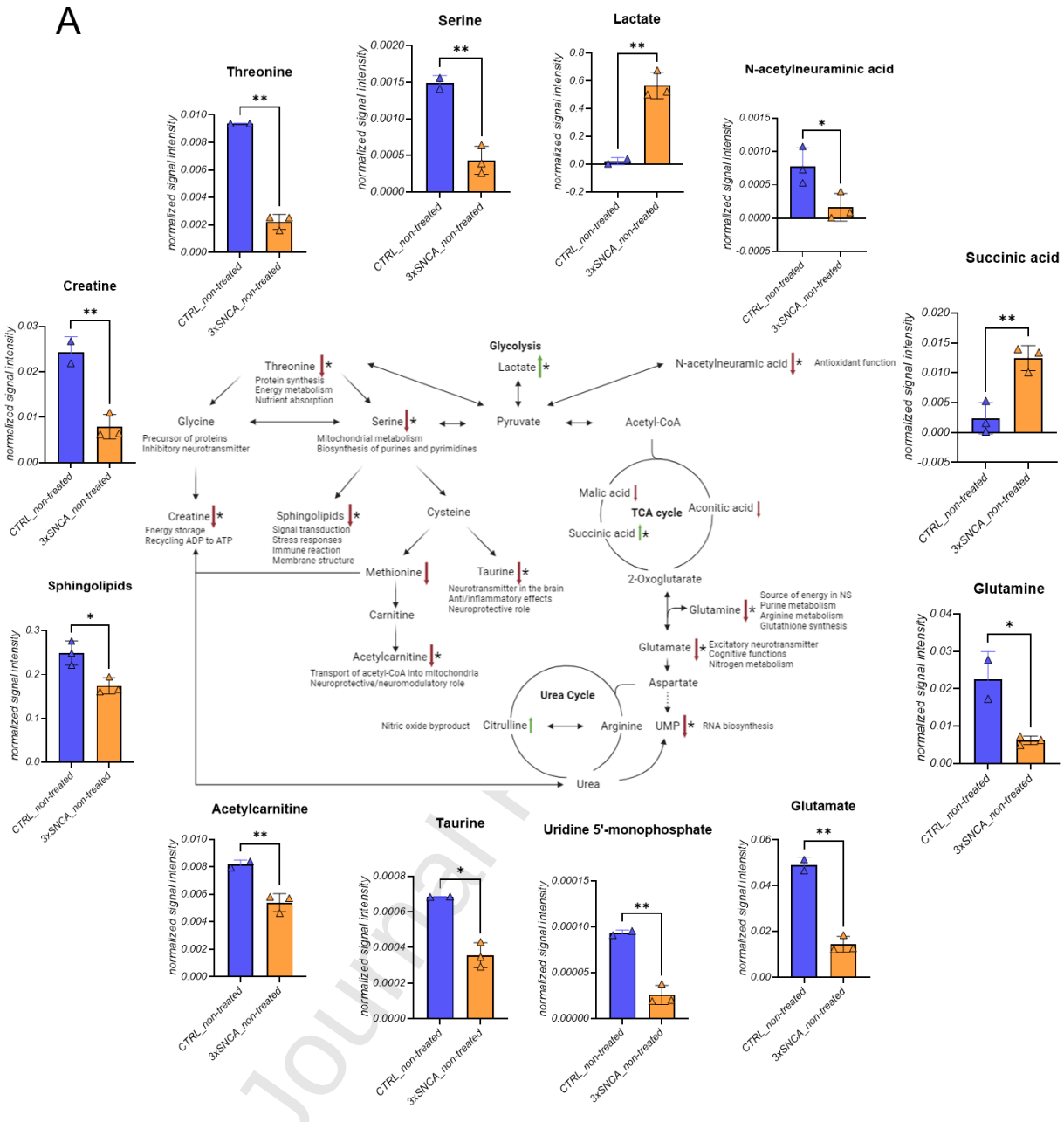

B

Metabolites	Fold change 3x*SNCA*/CTRL line	p-value (t-test)
N-acetylneuraminic acid	0.212	0.041
Threonine	0.237	0.002
Glutamine	0.274	0.026
Uridine 5'-monophosphate	0.276	0.004
Serine	0.29	0.004
Glutamate	0.295	0.005
Creatine	0.325	0.009
Taurine	0.521	0.015
Acetylcarnitine	0.659	0.008
Sphingolipids	0.699	0.022
Succinic acid	5.25	0.008
Lactate	25.824	0.006

Figure 7. Metabolites changing between CTRL and 3xSNCA hiPSC-derived neurons and their proposed involvement in metabolic pathways. *A) Detected metabolites were linked indicating bioenergetics processes and "branch points", where changes in PD (3xSNCA) cells occur. Particularly, alterations in the pathway involving threonine, serine, creatine and acetylcarnitine may result in impaired mitochondrial functioning given their crucial role in mitochondrial activities. Similarly, reduction in Krebs cycle metabolites and*

downstream metabolites such as glutamine and glutamate may be associated to oxidative stress and consequent cell damage. Black arrows indicate the progression of the pathway, with double arrows indicating that the metabolite can be derived from both directions; red arrows indicate decreased metabolites, while green arrows indicate increased metabolites in the PD line compared to the control line. Bar graphs represent normalized signal intensities for selected metabolites in the control (CTRL) and PD-derived (3xSNCA) cell lines. Asterisks indicate metabolites that were significantly different between the two lines. B) Table reporting the metabolites that were significantly different between CTRL and 3xSNCA with their respective fold change (3xSNCA/CTRL) and p-values.

Discussion

In this work, we examined the linkage between iron and dopamine metabolism in SH-SY5Y neuroblastoma cells and hiPSC-derived dopaminergic neurons. We observed that dopamine affects iron homeostasis, mitochondrial respiration, and oxidative stress by altering crucial iron transporters, leading to perturbations of intracellular and mitochondrial iron levels. These dopamine-induced alterations of iron homeostasis can result in the observed alterations of mitochondrial function (Lane et al., 2015; Oexle et al., 1999). Similarly, changes of intracellular iron metabolism, oxygen consumption, and mitochondrial metabolism were observed in healthy control hiPSC-derived dopaminergic neurons upon dopamine treatment. In contrast, in hiPSC-derived PD patient neurons, characterized by changes in iron homeostasis, dopamine promoted a beneficial effect by improving mitochondrial functionality.

Treatment with dopamine for 16 hours resulted in cellular damage, including decreased mitochondrial respiration and related mitochondrial alterations (reduced mtDNA copy number and citrate synthase activity), increased oxidative stress, and reduced iron-dependent aconitase activity, features observed both in SH-SY5Y neuroblastoma cells and in control hiPSC-derived neurons. Dopamine may therefore push the cells to the limits of their antioxidation/detoxification capacity when supplemented in excess. These data agree with the observation of Burbulla and colleagues, who described that Levodopa treatment, the precursor to dopamine that is used as a dopamine replacement agent in PD, was able to increase oxidized dopamine levels in human control neurons (Burbulla et al., 2017).

In SH-SY5Y cells, we found that dopamine treatment increased TFR1 expression both on mRNA and protein levels. The promotion of iron uptake induced by dopamine may be further related to a direct interaction between these two compounds, resulting in the formation of dopamine quinones and an increased cytoplasmic retention of iron as labile iron pool, more prone to oxidative events. This is in line with the chemical structure of dopamine bearing a catechol, a known iron-binding moiety (Zhang et al., 2020). Binding of iron to dopamine might result in a dysregulated iron homeostasis. Alternatively, iron might promote dopamine oxidation leading to toxic products such as aminochrome (Aguirre et al., 2012; Sun et al., 2018). In addition to these possibilities, accumulated iron can damage mitochondria via the Fenton reaction (Cerri et al., 2019; Ward et al., 2014) or by activating inflammatory molecules such as TNF-α and IL-6 (Martin-Bastida et al., 2021). Iron retention in the cytoplasm upon dopamine supplementation is further indicated by stable

FTH levels and no upregulation of FPN protein levels, although it was increased on the mRNA level (Tian et al., 2020; Zhang et al., 2020).

Since dopamine affects iron levels, the function of iron-sulfur-cluster containing enzymes such as ACO1 and ACO2 may be affected due to altered iron levels or oxidative stress (Pantopoulos et al., 1997) resulting in decreased protein and activity levels of these enzymes. It is known that hydrogen peroxide or nitric oxide can disrupt the iron-sulfur cluster of ACO1 activating its iron regulatory protein 1 (IRP1) conformation. This promotes intracellular iron accumulation by increasing TFR1 and DMT1 mRNA stability (Liu et al., 2022). Furthermore, superoxide anion, which we found increased upon dopamine treatment, was shown to inactivate ACO2 (Liang and Patel, 2004), suggesting that oxidative stress may decrease the activity of this enzyme, leading to a predicted repercussion on the cellular metabolism. Alternatively, iron loading can reduce ACO2 expression via IRP1 and 2 mediated translational repression (Muckenthaler et al., 2017). Dopamine-mediated damage of mitochondria was confirmed by reduced mitochondrial respiration, increased cytochrome *c* control efficiency, reduced mtDNA copy number, and reduced citrate synthase activity. Indeed, excessive free radical products created during energy production and dopamine metabolism can lead to damage of both mtDNA and the overall mitochondrial machinery (Swerdlow et al., 1996; Yan et al., 2013). Even though iron administered alone showed little effects on mitochondrial function, dopamine-caused impairments on mitochondria could not be overcome by concomitant substitution of iron.

Contrarily, in PD patient derived hiPSC-neurons with a 3x*SNCA* mutation, dopamine treatment led to a rescue effect shown by improved respiration, activation of antioxidant pathways (shown by SOD2 levels), and a series of positive effects on metabolites involved in mitochondrial function. In a recent work, it has been found that tetrahydrobiopterin (BH4) protected from genetically and chemically induced PD-related stressors in mice and human neurons from PD patients (Cronin et al., 2023). BH4 is an essential co-factor for enzymes involved in various cellular processes, for instance nitric oxide production, phenylalanine metabolism, and neurotransmitter biosynthesis, including dopamine synthesis (Werner et al., 2011). Cronin and colleagues observed that BH4 enhanced mitochondrial fitness and maintained firing rates of dopaminergic neurons (Cronin et al. 2023). In our model, comparable effects were fulfilled by dopamine administration. Furthermore, BH4 plays a role in preventing ferroptosis (Cronin et al., 2019). Likewise, dopamine may prevent ferroptosis by correcting iron imbalances in human dopaminergic neurons of PD models. Of note, a recent clinical study using the iron chelator deferiprone (DFP) to target pathological iron accumulation in patients with early onset PD failed to show clinical benefit and even resulted in worsening of symptoms (Devos et al., 2022). This points to the importance of spatio-temporal distribution of iron and dopamine for maintaining essential function.

When comparing non-treated neurons, higher TFR1 and lower FPN levels in the hiPSC-derived patient neurons suggested cytoplasmic iron deficiency opposite to evidence of mitochondrial iron accumulation, as reflected by higher MFRN2. However, while the combination of dopamine with $FeCl_3$ significantly decreased

TFR1 levels in the control line, treatments in the patient line – at least after 16 hours – did not affect TFR1 protein levels. This is in line with a shift of iron from the cytoplasm to mitochondria thereby prohibiting a prolonged increase of cytoplasmic iron levels, which could affect TFR expression via IRP/IRE interaction. Significant variations of FPN and FTH only in the control line after treatments further suggested that the two lines responded differently to perturbations of iron homeostasis. Failure in storage regulation with consequently increased levels of labile iron, as opposed to ferritin-bound iron, is known as a possible cause of iron-related cellular dysfunctions in PD (Tian et al., 2020). If free iron content is elevated, the Fenton reaction can generate ROS and therefore promote oxidative damage (Cheng et al., 2022). Accordingly, we found that SOD2 levels responded to dopamine treatment by alleviating mitochondrial oxidative stress in our PD model. Our data further suggested impaired iron handling in the PD neurons, in which mitochondrial iron overload may be prevented by dopamine treatment, for example by shuttling excess iron out of mitochondria. Moreover, in line with well-established mitochondrial defects, we measured decreased respiration in the 3x*SNCA* patient neurons compared to the control neurons. Multiple biological mechanisms may underlie this phenotype including a possible accumulation of α-syn in the PD neurons, increased amounts of oxidized dopamine (Burbulla et al., 2017), or iron overload (Fischer et al., 2021; Huang et al., 2018). Physiological responses to impaired mitochondria include a compensatory increase of transcription of PGC-1α, the major regulator of mitochondrial biogenesis (Lin et al., 2009). In contrast to control neurons, treatment of patient neurons with dopamine increased PGC-1α, underscoring again the beneficial effect of dopamine treatment in the PD model, which is in line with the observation of ameliorated mitochondrial function in restless legs syndrome subjects receiving Levodopa (Haschka et al., 2019). Interestingly, a recent study has investigated the *in vivo* effect of 200/50 mg levodopa/benserazide on mitochondrial bioenergetics in PD patients and matched healthy controls by ^{31}phosphorus magnetic resonance spectroscopy of the basal ganglia and the midbrain. This study detected bioenergetics defects in the basal ganglia but not in the midbrain of both groups suggesting an effect of dopamine only at that specific site of action (Prasuhn et al., 2024).

Of importance, an untargeted metabolomics approach revealed that most of the observed changes in the metabolism between the control and the PD patient neurons are attributable to energy/mitochondrial metabolism (e.g., threonine, serine pathways) and antioxidant mechanisms (e.g., glutamine). Glutamine is the precursor of glutamate and glutathione, a crucial antioxidant in the body (Lau and Tymianski, 2010; Zhang et al., 2019). Reduced levels of glutamine and glutamate in baseline conditions in the PD line may indicate their consumption to produce glutathione, and therefore to neutralize oxidative stress. The effect of dopamine on increasing these metabolite levels in the PD neurons but not in control neurons might be an indication of a compensatory reaction to underlying intrinsic oxidative stress. Notably, we also found reduced serine levels in the PD patient-derived neurons. L-serine plays an important role in essential neurometabolic processes, while its enantiomer, D-serine, is a potent co-agonist of the N-methyl-D-aspartate (NMDA)

receptor of glutamate, the principal excitatory neurotransmitter in the human brain (Di Maio et al., 2023). A recent study found increased levels of serine enantiomers (D- and L-serine) in *post mortem* samples from the caudate putamen and in the cerebrospinal fluid of living PD patients compared to controls (Di Maio et al., 2023). These data were resembled in another study in an MPTP (1-methyl- 4-phenyl-1, 2, 3, 6-tetrahydropyridine)-treated macaque model of PD, characterized by a severe dopaminergic degeneration, in which serine enantiomer levels were increased in a region-specific manner in the rostral putamen, but not in the subthalamic nucleus and the globus pallidus. These perturbations in the striatum were dependent on the level of dopaminergic degeneration, as they were not observed in MPTP-probenecid-treated mice, which showed only mild dopaminergic neurodegeneration (Serra et al., 2023). Furthermore, in the *substantia nigra* of MPTP-treated monkeys, reduced D-serine levels were detected (Nuzzo et al., 2019), which might be in line with the lower serine levels detected in our patient-derived neuronal cultures, although we did not measure serine levels with chiral resolution and were therefore not able to distinguish the two serine enantiomers. We observed reduced levels for both glutamine and glutamate, while their levels remained unchanged in the striatum of the MPTP-treated monkeys. Although the underlying mechanism of these region-specific amino acid alterations is still unknown, these previous studies and our data further highlight a different spatiotemporal functional distribution of these amino acids in the context of PD.

Several TCA metabolites, including malic acid and aconitic acid, were found reduced in PD neurons compared to the control cells, in line with the previously observed reduction in TCA cycle metabolites in PD (Shao and Le, 2019). Increased lactate levels in PD neurons point to the conversion of glucose to lactate during anaerobic glycolysis to compensate for a lack of ATP production in the TCA cycle. Succinic acid was found increased as described previously (Zambon et al., 2019). Beyond its production in the TCA cycle, succinate is also formed upon degradation of odd-chain fatty acids, methionine, threonine, leucine, or isoleucine. All these metabolites are finally converted to succinate with propionyl-CoA, methylmalonyl-CoA and succinyl-CoA as intermediates (Collado et al., 2020). Along with decreased levels of these precursors (methionine, threonine), we also observed an increase of propionylcarnitine and the ratio propionylcarnitine/acetylcarnitine in the patient line compared to the control line. Propionylcarnitine accumulation might indicate abnormalities in propionate catabolism or its excess production (confirmed also by its ratio), where excess propionate is transferred to carnitine to reduce its toxicity (Collado et al., 2020; Wongkittichote et al., 2019). In previous studies, short-chain fatty acids (SCFA) and the propionate pathway have been found to be dysregulated in PD (Chen et al., 2022; He et al., 2021; Levin et al., 2010; Park et al., 2017; Qi et al., 2023). Although there is controversy about the content of acetic acid and propionic acid (Qi et al., 2023), and these studies are conducted on serum or stool, increased levels of SCFAs, including propionic acid, were found in serum of PD patients compared to controls (Chen et al., 2022), confirming also previously observed results (He et al., 2021). Interestingly, plasma levels of propionic acid were associated to more severe motor symptoms (Chen et al., 2022). Moreover, elevated levels of methylmalonate and

homocysteine were observed in PD (Levin et al., 2010) suggesting that both might be markers for neurodegenerative processes, and both are linked to propionate metabolism. Furthermore, in serum, methylmalonic acid correlated with neuropathic pain in PD (Park et al., 2017), and low vitamin B12 levels, which is a master regulator of this pathway, are associated with a worse prognosis of PD, demyelination and peripheral neuropathy (Cardoso, 2018). Overall, dopamine treatment induced an opposite effect in the control neurons compared to PD patient neurons for some of the analyzed metabolites (threonine, serine, and glutamine pathway), pointing to a damaging effect of dopamine in control neurons and a beneficial effect in patient neurons by modifying these metabolic pathways.

Even though this work shows an important role for the dopamine-iron-mitochondria interplay in neuronal cell models, additional aspects of the biological mechanisms underlying the rescue of PD patient cells in relation to iron-mitochondrial homeostasis await further clarification. For instance, we measured mRNA and protein expression at a single time point and may thus have missed early changes or detected the sum of dopamine-mediated alterations and counter regulatory signals. In hiPSC-derived neurons, mRNA and protein expression were assessed in mature neurons at day 60 of differentiation, while oxygen consumption was measured at day 35. However, although neurons at earlier time point may not have reached the mature neuronal stage, we have shown previously that they express the dopaminergic neuron markers TH and DAT and show alterations of mitochondrial function caused by mutations in the *SNCA* and *PRKN* genes (Castelo Rueda et al., 2023; Gilmozzi et al., 2021). Furthermore, antibiotics such as streptomycin and penicillin can induce mitochondrial proteotoxic stress in cell cultures with potential effects on the study results (Wang et al., 2015). To expand these studies on the effect of dopaminergic treatment on iron-mitochondria biochemical pathways, the investigation of additional iPSC-lines, most importantly derived from idiopathic PD patients, representing the vast majority of PD patients, as well as establishment of co-cultures/organoids of dopaminergic neurons with other neuronal and glial cell populations or *in vivo* studies (e.g. MPTP-mouse model) might help to reconstitute a more physiological environment.

Conclusions

In conclusion, the present study found that altered iron homeostasis may contribute to mitochondrial dysfunction observed in PD and that treatment with dopamine beneficially affects iron-mitochondria biochemical pathways. Based on the collected data, we hypothesize that, under physiological conditions, dopamine may constitute a complex with iron in the extracellular environment, shuttle it across membranes, and promote mitochondrial dysfunction and ROS production. In contrast, in PD-neurons, characterized by intracellular iron-misdistribution and mitochondrial dysfunction, administration of dopamine may partially restore altered intracellular and mitochondrial iron distribution by shuttling iron between cytoplasm and mitochondria and thus rescue mitochondrial dysfunction. A further dissection of these interactions and their involvement in PD pathogenesis might be useful for the development of targeted therapeutic approaches

able to restore altered intracellular iron distribution and to prevent the formation of oxidative stress as a means of limiting neuronal injury in PD.

DECLARATIONS

Ethics approval and consent to participate and t for publication

The study was approved by the Ethics Committee of the Healthcare System of the Autonomous Province of Bozen/Bolzano (approval number 102-2014 dated 26.11.2014 with extension from 19.02.2020). Study participants provided their written informed consent to participate in this study. Study participants have given their consent for publication in an anonymous form.

Availability of data and material

All data generated during this study are included in this article and its supplementary information file. As for the metabolomics data, the informed consent provided by the study participants does not allow the upload of individual-level metabolomic data to public repositories.

Competing interests

All authors declare no competing interests.

Funding

This research was funded by the Department of Innovation, Research, University, and Museums of the Autonomous Province of Bozen/Bolzano, Italy, through a core funding initiative to the Institute for Biomedicine and by the bilateral (Bi-Doc) doctoral programme between the Medical University of Innsbruck, Austria and Eurac Research in Bolzano, Italy. This work was supported by a grant from the Christian Doppler Society, Austria to GW. Moreover, PPP was supported by the Deutsche Forschungsgemeinschaft (FOR2488). The stage of CB at LCSB was funded by Erasmus+ and the KWA program of the Medical University of Innsbruck. BTA is part of the “Microbiomes in One Health” PhD training program, which is supported by the PRIDE doctoral research funding scheme (PRIDE/11823097) of the Luxembourg National Research Fund (FNR). ELS acknowledges funding support from the FNR for project A18/BM/12341006. CMG acknowledges support from the European Union’s Horizon 2020 Research and Innovation Programme under grant agreement No. 814418 (SinFonia). Sponsors did not have any role in study design, collection, analysis and interpretation of data, writing of the report, and in the decision to submit the article for publication.

Authors' contributions

CB: designed and performed experiments, analyzed the data and wrote the manuscript; MS: designed and performed experiments, reviewed the manuscript; ML: designed and performed experiments, analyzed the data, participated in the interpretation of results, wrote and revised the manuscript; CMG: provided support for the metabolomic analyses, revised the manuscript; BTA: provided support for the metabolomic analyses, revised the manuscript; MPCR: designed and performed experiments, revised the manuscript; CF: helped

with experiments and helped revise the manuscript; CD: provided support for Oxygraph experiments and revised the manuscript; HT: performed the atomic absorption spectroscopy experiments; AZ: designed and performed experiments, revised the manuscript; PPP: provided critical review of the manuscript; ELS: performed critical input and revised the manuscript; IP: designed and supervised the project, participated in the interpretation of results, wrote and revised the manuscript; GW: designed and supervised the project, provided the interpretation of results, wrote and revised the manuscript.
All authors read and approved the final manuscript.

Acknowledgements

The authors acknowledge the metabolomics platform of the LCSB and Lorenzo Favilli for the support during the LC-MS experiments and analysis. The authors also thank Giovanna Gentile, Valentina Gilmozzi, and Chiara Volani for experimental support and Gianfranco Frigerio for his help hosting the exchange at LCSB. CD has been employed by Oroboros Instruments.

References

Aguirre, P., et al., 2012. The dopamine metabolite aminochrome inhibits mitochondrial complex I and modifies the expression of iron transporters DMT1 and FPN1. Biometals. 25**,** 795-803, 10.1007/s10534-012-9525-y.

Ali, M. Y., et al., 2022. Mitoferrin, Cellular and Mitochondrial Iron Homeostasis. Cells. 11, 10.3390/cells11213464.

Antonyova, V., et al., 2020. Role of mtDNA disturbances in the pathogenesis of Alzheimer's and Parkinson's disease. DNA Repair (Amst). 91-92**,** 102871, 10.1016/j.dnarep.2020.102871.

Arreguin, S., et al., 2009. Dopamine complexes of iron in the etiology and pathogenesis of Parkinson's disease. J Inorg Biochem. 103**,** 87-93, 10.1016/j.jinorgbio.2008.09.007.

Beinert, H., Kennedy, M. C., 1993. Aconitase, a two-faced protein: enzyme and iron regulatory factor. FASEB J. 7**,** 1442-9, 10.1096/fasebj.7.15.8262329.

Bernal-Conde, L. D., et al., 2019. Alpha-Synuclein Physiology and Pathology: A Perspective on Cellular Structures and Organelles. Front Neurosci. 13**,** 1399, 10.3389/fnins.2019.01399.

Blauwendraat, C., et al., 2020. The genetic architecture of Parkinson's disease. Lancet Neurol. 19**,** 170-178, 10.1016/S1474-4422(19)30287-X.

Bloem, B. R., et al., 2021. Parkinson's disease. Lancet. 397**,** 2284-2303, 10.1016/S0140-6736(21)00218-X.

Bolton, E., et al., Pubchemlite for Exposomics. Zenodo, 2023, https://doi.org/10.5281/zenodo.7788370.

Burbulla, L. F., et al., 2017. Dopamine oxidation mediates mitochondrial and lysosomal dysfunction in Parkinson's disease. Science. 357**,** 1255-1261, 10.1126/science.aam9080.

Cajka, T., et al., 2017. Validating Quantitative Untargeted Lipidomics Across Nine Liquid Chromatography-High-Resolution Mass Spectrometry Platforms. Anal Chem. 89**,** 12360-12368, 10.1021/acs.analchem.7b03404.

Cardoso, F., 2018. Vitamin B12 and Parkinson's Disease: What is the Relationship? Mov Disord. 33**,** 702-703, 10.1002/mds.27366.

Castelo Rueda, M. P., et al., 2023. Molecular phenotypes of mitochondrial dysfunction in clinically non-manifesting heterozygous PRKN variant carriers. NPJ Parkinsons Dis. 9**,** 65, 10.1038/s41531-023-00499-9.

Cerri, S., et al., 2019. Endocytic iron trafficking and mitochondria in Parkinson's disease. Int J Biochem Cell Biol. 110**,** 70-74, 10.1016/j.biocel.2019.02.009.

Chang, D., et al., 2017. A meta-analysis of genome-wide association studies identifies 17 new Parkinson's disease risk loci. Nat Genet. 49**,** 1511-1516, 10.1038/ng.3955.

Chartier-Harlin, M. C., et al., 2004. Alpha-synuclein locus duplication as a cause of familial Parkinson's disease. Lancet. 364**,** 1167-9, 10.1016/S0140-6736(04)17103-1.

Chen, S. J., et al., 2022. Association of Fecal and Plasma Levels of Short-Chain Fatty Acids With Gut Microbiota and Clinical Severity in Patients With Parkinson Disease. Neurology. 98**,** e848-e858, 10.1212/WNL.0000000000013225.

Cheng, R., et al., 2022. Mitochondrial iron metabolism and neurodegenerative diseases. Neurotoxicology. 88**,** 88-101, 10.1016/j.neuro.2021.11.003.

Cheung, Y.-T., et al., 2009. Effects of all-trans-retinoic acid on human SH-SY5Y neuroblastoma as in vitro model in neurotoxicity research. Neurotoxicology 30, 127–135, 10.1016/j.neuro.2008.11.001

Choi, M. L., et al., 2022. Pathological structural conversion of alpha-synuclein at the mitochondria induces neuronal toxicity. Nat Neurosci. 25**,** 1134-1148, 10.1038/s41593-022-01140-3.

Ci, Y. Z., et al., 2020. Iron overload induced by IRP2 gene knockout aggravates symptoms of Parkinson's disease. Neurochem Int. 134**,** 104657, 10.1016/j.neuint.2019.104657.

Collaborators, G. B. D. P. s. D., 2018. Global, regional, and national burden of Parkinson's disease, 1990-2016: a systematic analysis for the Global Burden of Disease Study 2016. Lancet Neurol. 17**,** 939-953, 10.1016/S1474-4422(18)30295-3.

Collado, M. S., et al., 2020. Biochemical and anaplerotic applications of in vitro models of propionic acidemia and methylmalonic acidemia using patient-derived primary hepatocytes. Mol Genet Metab. 130**,** 183-196, 10.1016/j.ymgme.2020.05.003.

Cronin, S. J. F., et al., 2019. The Role of Iron Regulation in Immunometabolism and Immune-Related Disease. Front Mol Biosci. 6**,** 116, 10.3389/fmolb.2019.00116.

Cronin, S. J. F., et al., 2023. Crucial neuroprotective roles of the metabolite BH4 in dopaminergic neurons. bioRxiv. 10.1101/2023.05.08.539795.

David, S., et al., 2022. Dysregulation of Iron Homeostasis in the Central Nervous System and the Role of Ferroptosis in Neurodegenerative Disorders. Antioxid Redox Signal. 37**,** 150-170, 10.1089/ars.2021.0218.

Devos, D., et al., 2022. Trial of Deferiprone in Parkinson's Disease. N Engl J Med. 387**,** 2045-2055, 10.1056/NEJMoa2209254.

Dias, V., et al., 2013. The role of oxidative stress in Parkinson's disease. J Parkinsons Dis. 3**,** 461-91, 10.3233/JPD-130230.

Dichtl, S., et al., 2019. Dopamine Is a Siderophore-Like Iron Chelator That Promotes Salmonella enterica Serovar Typhimurium Virulence in Mice. mBio. 10, 10.1128/mBio.02624-18.

Dichtl, S., et al., 2018. Dopamine promotes cellular iron accumulation and oxidative stress responses in macrophages. Biochem Pharmacol. 148**,** 193-201, 10.1016/j.bcp.2017.12.001.

Di Maio, A., et al., 2023. Homeostasis of serine enantiomers is disrupted in the post-mortem caudate putamen and cerebrospinal fluid of living Parkinson's disease patients. Neurobiol Dis 184, 106203, 10.1016/j.nbd.2023.106203

Doerrier, C., et al., 2018. High-Resolution FluoRespirometry and OXPHOS Protocols for Human Cells, Permeabilized Fibers from Small Biopsies of Muscle, and Isolated Mitochondria. Methods Mol Biol. 1782**,** 31-70, 10.1007/978-1-4939-7831-1_3.

Fischer, C., et al., 2021. Dietary Iron Overload and Hfe(-/-) Related Hemochromatosis Alter Hepatic Mitochondrial Function. Antioxidants (Basel). 10, 10.3390/antiox10111818.

Forno, L. S., 1996. Neuropathology of Parkinson's disease. J Neuropathol Exp Neurol. 55**,** 259-72, 10.1097/00005072-199603000-00001.

Gao, G., et al., 2019. Cellular Iron Metabolism and Regulation. Adv Exp Med Biol. 1173**,** 21-32, 10.1007/978-981-13-9589-5_2.

Gilmozzi, V., et al., 2021. Generation of hiPSC-Derived Functional Dopaminergic Neurons in Alginate-Based 3D Culture. Front Cell Dev Biol 9, 708389, 10.3389/fcell.2021.708389

Goetz, D. H., et al., 2002. The neutrophil lipocalin NGAL is a bacteriostatic agent that interferes with siderophore-mediated iron acquisition. Mol Cell. 10**,** 1033-43, 10.1016/s1097-2765(02)00708-6.

Gomez-Giro, G., et al., 2019. Synapse alterations precede neuronal damage and storage pathology in a human cerebral organoid model of CLN3-juvenile neuronal ceroid lipofuscinosis. Acta Neuropathol Commun. 7**,** 222, 10.1186/s40478-019-0871-7.

Grunewald, A., et al., 2019. New insights into the complex role of mitochondria in Parkinson's disease. Prog Neurobiol. 177**,** 73-93, 10.1016/j.pneurobio.2018.09.003.

Hare, D. J., Double, K. L., 2016. Iron and dopamine: a toxic couple. Brain. 139**,** 1026-35, 10.1093/brain/aww022.

Haschka, D., et al., 2019. Association of mitochondrial iron deficiency and dysfunction with idiopathic restless legs syndrome. Mov Disord. 34**,** 114-123, 10.1002/mds.27482.

He, X., et al., 2021. Plasma Short-Chain Fatty Acids Differences in Multiple System Atrophy from Parkinson's Disease. J Parkinsons Dis. 11**,** 1167-1176, 10.3233/JPD-212604.

Huang, X. T., et al., 2018. Iron-induced energy supply deficiency and mitochondrial fragmentation in neurons. J Neurochem. 147**,** 816-830, 10.1111/jnc.14621.

Jager, C., et al., 2016. Metabolic Profiling and Quantification of Neurotransmitters in Mouse Brain by Gas Chromatography-Mass Spectrometry. Curr Protoc Mouse Biol. 6**,** 333-342, 10.1002/cpmo.15.

Jellinger, K., et al., 1990. Brain iron and ferritin in Parkinson's and Alzheimer's diseases. J Neural Transm Park Dis Dement Sect. 2**,** 327-40, 10.1007/BF02252926.

Joppe, K., et al., 2019. The Contribution of Iron to Protein Aggregation Disorders in the Central Nervous System. Front Neurosci. 13**,** 15, 10.3389/fnins.2019.00015.

Kaindlstorfer, C., et al., 2018. The Relevance of Iron in the Pathogenesis of Multiple System Atrophy: A Viewpoint. J Alzheimers Dis. 61**,** 1253-1273, 10.3233/JAD-170601.

Koskenkorva-Frank, T. S., et al., 2013. The complex interplay of iron metabolism, reactive oxygen species, and reactive nitrogen species: insights into the potential of various iron therapies to induce oxidative and nitrosative stress. Free Radic Biol Med. 65**,** 1174-1194, 10.1016/j.freeradbiomed.2013.09.001.

Kriks, S., et al., 2011. Dopamine neurons derived from human ES cells efficiently engraft in animal models of Parkinson's disease. Nature. 480**,** 547-51, 10.1038/nature10648.

Kuhn, D. M., et al., 2004. Nitrotyrosine as a marker for peroxynitrite-induced neurotoxicity: the beginning or the end of the end of dopamine neurons? J Neurochem. 89**,** 529-36, 10.1111/j.1471-4159.2004.02346.x.

Lane, D. J., et al., 2015. Cellular iron uptake, trafficking and metabolism: Key molecules and mechanisms and their roles in disease. Biochim Biophys Acta. 1853**,** 1130-44, 10.1016/j.bbamcr.2015.01.021.

Lang, M., et al., 2022. A genome on shaky ground: exploring the impact of mitochondrial DNA integrity on Parkinson's disease by highlighting the use of cybrid models. Cell Mol Life Sci. 79**,** 283, 10.1007/s00018-022-04304-3.

Lau, A., Tymianski, M., 2010. Glutamate receptors, neurotoxicity and neurodegeneration. Pflugers Arch. 460**,** 525-42, 10.1007/s00424-010-0809-1.

Lemieux, H., et al., 2017. Remodeling pathway control of mitochondrial respiratory capacity by temperature in mouse heart: electron flow through the Q-junction in permeabilized fibers. Sci Rep. 7**,** 2840, 10.1038/s41598-017-02789-8.

Levin, J., et al., 2010. Elevated levels of methylmalonate and homocysteine in Parkinson's disease, progressive supranuclear palsy and amyotrophic lateral sclerosis. Dement Geriatr Cogn Disord. 29**,** 553-9, 10.1159/000314841.

Lhermitte, J., et al., 1924. Original Papers: ON THE OCCURRENCE OF ABNORMAL DEPOSITS OF IRON IN THE BRAIN IN PARKINSONISM WITH SPECIAL REFERENCE TO ITS LOCALISATION. J Neurol Psychopathol. 5**,** 195-208, 10.1136/jnnp.s1-5.19.195.

Li, S. W., et al., 2016. Iron overload induced by ferric ammonium citrate triggers reactive oxygen species-mediated apoptosis via both extrinsic and intrinsic pathways in human hepatic cells. Hum Exp Toxicol. 35**,** 598-607, 10.1177/0960327115597312.

Liang, L. P., Patel, M., 2004. Iron-sulfur enzyme mediated mitochondrial superoxide toxicity in experimental Parkinson's disease. J Neurochem. 90**,** 1076-84, 10.1111/j.1471-4159.2004.02567.x.

Lill, R., Freibert, S. A., 2020. Mechanisms of Mitochondrial Iron-Sulfur Protein Biogenesis. Annu Rev Biochem. 89**,** 471-499, 10.1146/annurev-biochem-013118-111540.

Lin, T. K., et al., 2009. Mitochondrial dysfunction and biogenesis in the pathogenesis of Parkinson's disease. Chang Gung Med J. 32**,** 589-99,

Liu, R. Z., et al., 2022. Baicalein Attenuates Brain Iron Accumulation through Protecting Aconitase 1 from Oxidative Stress in Rotenone-Induced Parkinson's Disease in Rats. Antioxidants (Basel). 12, 10.3390/antiox12010012.

Ma, L., et al., 2021. Parkinson's disease: Alterations in iron and redox biology as a key to unlock therapeutic strategies. Redox Biol. 41**,** 101896, 10.1016/j.redox.2021.101896.

Malpartida, A. B., et al., 2021. Mitochondrial Dysfunction and Mitophagy in Parkinson's Disease: From Mechanism to Therapy. Trends Biochem Sci. 46**,** 329-343, 10.1016/j.tibs.2020.11.007.

Marras, C., et al., 2016. Nomenclature of genetic movement disorders: Recommendations of the international Parkinson and movement disorder society task force. Mov Disord. 31**,** 436-57, 10.1002/mds.26527.

Martin-Bastida, A., et al., 2021. Iron and inflammation: in vivo and post-mortem studies in Parkinson's disease. J Neural Transm (Vienna). 128**,** 15-25, 10.1007/s00702-020-02271-2.

Matak, P., et al., 2016. Disrupted iron homeostasis causes dopaminergic neurodegeneration in mice. Proc Natl Acad Sci U S A. 113**,** 3428-35, 10.1073/pnas.1519473113.

Mercuri, N. B., et al., 2000. Tranylcypromine, but not moclobemide, prolongs the inhibitory action of dopamine on midbrain dopaminergic neurons: an in vitro electrophysiological study. Synapse. 37**,** 216-21, 10.1002/1098-2396(20000901)37:3<216::AID-SYN5>3.0.CO;2-3.

Miyazaki, I., Asanuma, M., 2008. Dopaminergic neuron-specific oxidative stress caused by dopamine itself. Acta Med Okayama. 62**,** 141-50, 10.18926/AMO/30942.

Monzio Compagnoni, G., et al., 2020. The Role of Mitochondria in Neurodegenerative Diseases: the Lesson from Alzheimer's Disease and Parkinson's Disease. Mol Neurobiol. 57**,** 2959-2980, 10.1007/s12035-020-01926-1.

Muckenthaler, M. U., et al., 2017. A Red Carpet for Iron Metabolism. Cell. 168**,** 344-361, 10.1016/j.cell.2016.12.034.

Muhlenhoff, U., et al., 2015. Compartmentalization of iron between mitochondria and the cytosol and its regulation. Eur J Cell Biol. 94**,** 292-308, 10.1016/j.ejcb.2015.05.003.

Munoz, Y., et al., 2016. Parkinson's Disease: The Mitochondria-Iron Link. Parkinsons Dis. 2016**,** 7049108, 10.1155/2016/7049108.

Nuzzo, T., et al., 2019. The levels of the NMDA receptor co-agonist D-serine are reduced in the substantia nigra of MPTP-lesioned macaques and in the cerebrospinal fluid of Parkinson's disease patients. Sci Rep 9, 8898, 10.1038/s41598-019-45419-1

Oexle, H., et al., 1999. Iron-dependent changes in cellular energy metabolism: influence on citric acid cycle and oxidative phosphorylation. Biochim Biophys Acta. 1413**,** 99-107, 10.1016/s0005-2728(99)00088-2.

Ortega, R., et al., 2016. alpha-Synuclein Over-Expression Induces Increased Iron Accumulation and Redistribution in Iron-Exposed Neurons. Mol Neurobiol. 53**,** 1925-1934, 10.1007/s12035-015-9146-x.

Pantopoulos, K., et al., 1997. Differences in the regulation of iron regulatory protein-1 (IRP-1) by extra- and intracellular oxidative stress. J Biol Chem. 272**,** 9802-8, 10.1074/jbc.272.15.9802.

Parihar, M. S., et al., 2008. Mitochondrial association of alpha-synuclein causes oxidative stress. Cell Mol Life Sci. 65**,** 1272-84, 10.1007/s00018-008-7589-1.

Park, J. S., et al., 2018. Mitochondrial Dysfunction in Parkinson's Disease: New Mechanistic Insights and Therapeutic Perspectives. Curr Neurol Neurosci Rep. 18**,** 21, 10.1007/s11910-018-0829-3.

Park, J. S., et al., 2017. Serum methylmalonic acid correlates with neuropathic pain in idiopathic Parkinson's disease. Neurol Sci. 38**,** 1799-1804, 10.1007/s10072-017-3056-9.

Post, B., et al., 2020. Young Onset Parkinson's Disease: A Modern and Tailored Approach. J Parkinsons Dis. 10**,** S29-S36, 10.3233/JPD-202135.

Prasuhn, J., et al., 2024. Levodopa Impairs the Energy Metabolism of the Basal Ganglia In Vivo. Ann Neurol., 10.1002/ana.26884

Pringsheim, T., et al., 2014. The prevalence of Parkinson's disease: a systematic review and meta-analysis. Mov Disord. 29**,** 1583-90, 10.1002/mds.25945.

Qi, A., et al., 2023. Plasma Metabolic Analysis Reveals the Dysregulation of Short-Chain Fatty Acid Metabolism in Parkinson's Disease. Mol Neurobiol. 60**,** 2619-2631, 10.1007/s12035-022-03157-y.

Riederer, P., et al., 1989. Neurochemical perspectives to the function of monoamine oxidase. Acta Neurol Scand Suppl. 126**,** 41-5, 10.1111/j.1600-0404.1989.tb01781.x.

Rouault, T. A., 2006. The role of iron regulatory proteins in mammalian iron homeostasis and disease. Nat Chem Biol. 2**,** 406-14, 10.1038/nchembio807.

Ruttkies, C., et al., 2016. MetFrag relaunched: incorporating strategies beyond in silico fragmentation. Journal of Cheminformatics. 8**,** 3, 10.1186/s13321-016-0115-9.

Schymanski, E. L., et al., 2014. Identifying small molecules via high resolution mass spectrometry: communicating confidence. Environ Sci Technol. 48**,** 2097-8, 10.1021/es5002105.

Schymanski, E. L., et al., 2021. Empowering large chemical knowledge bases for exposomics: PubChemLite meets MetFrag. J Cheminform. 13**,** 19, 10.1186/s13321-021-00489-0.

Serra, M., et al., 2023. Perturbation of serine enantiomers homeostasis in the striatum of MPTP-lesioned monkeys and mice reflects the extent of dopaminergic midbrain degeneration. Neurobiol Dis 184, 106226, 10.1016/j.nbd.2023.106226

Shao, Y., Le, W., 2019. Recent advances and perspectives of metabolomics-based investigations in Parkinson's disease. Mol Neurodegener. 14**,** 3, 10.1186/s13024-018-0304-2.

Shibasaki, Y., et al., 1995. High-resolution mapping of SNCA encoding alpha-synuclein, the non-A beta component of Alzheimer's disease amyloid precursor, to human chromosome 4q21.3-->q22 by fluorescence in situ hybridization. Cytogenet Cell Genet. 71**,** 54-5, 10.1159/000134061.

Spillantini, M. G., et al., 1998. alpha-Synuclein in filamentous inclusions of Lewy bodies from Parkinson's disease and dementia with lewy bodies. Proc Natl Acad Sci U S A. 95**,** 6469-73, 10.1073/pnas.95.11.6469.

Sulzer, D., et al., 2000. Neuromelanin biosynthesis is driven by excess cytosolic catecholamines not accumulated by synaptic vesicles. Proc Natl Acad Sci U S A. 97**,** 11869-74, 10.1073/pnas.97.22.11869.

Sun, Y., et al., 2018. Kinetic Modeling of pH-Dependent Oxidation of Dopamine by Iron and Its Relevance to Parkinson's Disease. Front Neurosci. 12**,** 859, 10.3389/fnins.2018.00859.

Swerdlow, R. H., et al., 1996. Origin and functional consequences of the complex I defect in Parkinson's disease. Ann Neurol. 40**,** 663-71, 10.1002/ana.410400417.

Talavera Andujar, B., et al., 2022. Studying the Parkinson's disease metabolome and exposome in biological samples through different analytical and cheminformatics approaches: a pilot study. Anal Bioanal Chem. 414**,** 7399-7419, 10.1007/s00216-022-04207-z.

Teppola, H., et al., 2016. Morphological Differentiation Towards Neuronal Phenotype of SH-SY5Y Neuroblastoma Cells by Estradiol, Retinoic Acid and Cholesterol. Neurochem Res 41, 731–47, 10.1007/s11064-015-1743-6

Theurl, I., et al., 2016. On-demand erythrocyte disposal and iron recycling requires transient macrophages in the liver. Nat Med. 22**,** 945-51, 10.1038/nm.4146.

Tian, Y., et al., 2020. FTH1 Inhibits Ferroptosis Through Ferritinophagy in the 6-OHDA Model of Parkinson's Disease. Neurotherapeutics. 17**,** 1796-1812, 10.1007/s13311-020-00929-z.

Tsugawa, H., et al., 2020. A lipidome atlas in MS-DIAL 4. Nature Biotechnology. 38**,** 1159-1163, 10.1038/s41587-020-0531-2.

Volani, C., et al., 2017. Dietary iron loading negatively affects liver mitochondrial function. Metallomics. 9**,** 1634-1644, 10.1039/c7mt00177k.

Wang, X., et al., 2015. Antibiotic use and abuse: a threat to mitochondria and chloroplasts with impact on research, health, and environment. Bioessays 37, 1045–53, 10.1002/bies.201500071

Ward, R. J., et al., 2014. The role of iron in brain ageing and neurodegenerative disorders. Lancet Neurol. 13**,** 1045-60, 10.1016/S1474-4422(14)70117-6.

Werner, E. R., et al., 2011. Tetrahydrobiopterin: biochemistry and pathophysiology. Biochem J. 438**,** 397-414, 10.1042/BJ20110293.

Wongkittichote, P., et al., 2019. Tricarboxylic acid cycle enzyme activities in a mouse model of methylmalonic aciduria. Mol Genet Metab. 128**,** 444-451, 10.1016/j.ymgme.2019.10.007.

Yan, M. H., et al., 2013. Mitochondrial defects and oxidative stress in Alzheimer disease and Parkinson disease. Free Radic Biol Med. 62**,** 90-101, 10.1016/j.freeradbiomed.2012.11.014.

Zambon, F., et al., 2019. Cellular alpha-synuclein pathology is associated with bioenergetic dysfunction in Parkinson's iPSC-derived dopamine neurons. Hum Mol Genet. 28**,** 2001-2013, 10.1093/hmg/ddz038.

Zanon, A., et al., 2017. SLP-2 interacts with Parkin in mitochondria and prevents mitochondrial dysfunction in Parkin-deficient human iPSC-derived neurons and Drosophila. Hum Mol Genet. 26**,** 2412-2425, 10.1093/hmg/ddx132.

Zhang, Y., et al., 2020. Iron Acquisition by Bacterial Pathogens: Beyond Tris-Catecholate Complexes. Chembiochem. 21**,** 1955-1967, 10.1002/cbic.201900778.

Zhang, Z., et al., 2019. Roles of Glutamate Receptors in Parkinson's Disease. Int J Mol Sci. 20, 10.3390/ijms20184391.

Zhou, Z. D., Tan, E. K., 2017. Iron regulatory protein (IRP)-iron responsive element (IRE) signaling pathway in human neurodegenerative diseases. Mol Neurodegener. 12**,** 75, 10.1186/s13024-017-0218-4.

Zucca, F. A., et al., 2017. Interactions of iron, dopamine and neuromelanin pathways in brain aging and Parkinson's disease. Prog Neurobiol. 155**,** 96-119, 10.1016/j.pneurobio.2015.09.012.

Graphical abstract

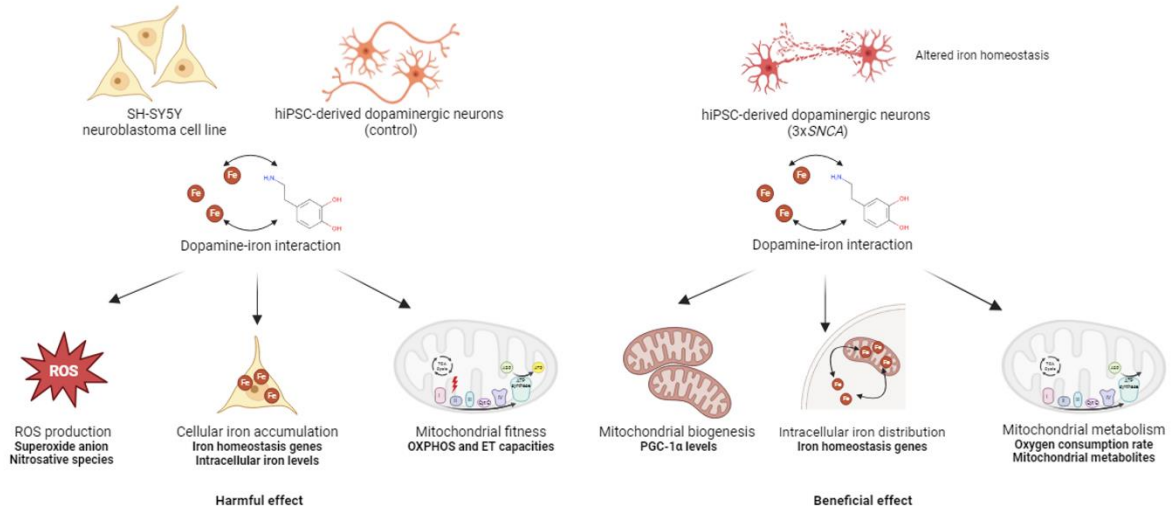

Highlights

- Dopamine alters iron homeostasis in neuronal cell models
- Mitochondria are susceptible to dopamine-iron interaction
- Dopamine-mediated iron perturbations induce oxidative stress under physiological conditions
- In a cellular model of Parkinson's disease, dopamine restores altered intracellular iron distribution and mitochondrial function